Design and Construction of a STM for use in-situ in a TEM

by Ben Medford

Thesis submitted to the University of Nottingham
for the degree of Master in Philosophy,
November 2009

Abstract

Since its inception scanning tunneling microscopy (STM) has emerged as a powerful technique in the field of nanoscience, with applications that have provided extremely important insights into the local nano-scale chemical/electrical properties of semiconducting and conducting materials[1]. However, this technique alone is not capable of directly observing the tip and sample during its operation. Direct observation of the dynamic changes of both the tip and sample may help to provide a better understanding of the mechanisms behind some STM applications. Recent developments in this area have successfully combined STM to operate in-situ with imaging techniques such as Scanning Electron Microscopy (SEM) and Transmission Electron Microscopy (TEM)[2].

This thesis presents a new design for an in-situ STM which can operate within the spatial confines of a TEM – allowing both techniques to be conducted simultaneously. To overcome the spatial constraints of imaging inside a TEM, the design uses a novel coarse approach mechanism; consisting of three parallel hammer-action inertial driving mechanisms[3] that are attached via flexible linkages to a pivot plate that allows the STM tip to be reliably positioned to regions of interest in three dimensions. The operation of STM in a TEM provides numerous advantages that are not available with standard STM techniques; these advantages are discussed and potential applications for this technique are also presented. One such application investigated is the potential for using silver sulphide STM tips for use in in-situ STM manipulation.

Acknowledgments

I would like to thank first and foremost my supervisor Professor Peter Beton for his guidance throughout this project. I would also like to thank Ben Rogers, Martin Humphrey and Richard Fawcett who have provided knowledge and essential practical advice. I express my gratitude to all the guys in the workshop: Bob Chettle, Steve Tabreham and especially Dave Laird – who has invested a huge amount of time and effort in the design and construction of the in-situ STM. Also deserving thanks are the entire Nottingham nanoscience department, for all the diverse information I've gained from them during my study here. And finally, I would like to thank all members of the Nanorobotics Research Group, especially Beverley Inkson, Günther Möbus, Ralf Gay, Yong Peng, Jing Jing Wang and Aiden Lockwood. This research group is a collaboration between the University of Nottingham, the University of Sheffield and Sheffield Hallam University; the group has always given helpful advice and provided me with access to essential equipment.

Contents

Chapter 1

Introduction

1.1. Nanoscience and Nanotechnology

From observation of the scientific and technological progress of the human race in recent years, it is evident that products are being manufactured at increasingly smaller scales; a trend known as “miniaturisation”. Perhaps the most obvious example of miniaturisation is in the field of computing. Early computers were extremely large[4], a complete contrast to the diminutive laptop computers of today. The discovery of the transistor, by Bardeen, Brattain and Shockley in 1947, set the miniaturisation of computers into motion - as bulky vacuum tubes used previously were replaced with integrated solid-state devices. This general trend of miniaturisation was subsequently highlighted by Gordon E. Moore[5] in 1965. He famously observed that the transistor density on integrated circuits doubled approximately every two years, and predicted the trend would continue. It did, and has continued to the present day, where transistors inside computers have been reduced to ~ nm in size.

At present computers are smaller than they have ever been, but what benefits have been gained from miniaturisation? In 1999, Bill Gates – then CEO of Microsoft - stated "Worldwide, well over 100 million personal computers will be sold this year. That means the world now buys almost as many personal computers as colour TVs"[6]. Without miniaturisation a household would realistically have to dedicate an entire room for each computer they possess. It is therefore unfeasible to think that computers could have become so popular among households and businesses. At present, we have handheld computing devices that allow us to listen to music, stream video from the internet and store huge amounts of information - all made possible by miniaturisation. However, is there really any added benefit further miniaturisation? From a scientific

and commercial viewpoint there is strong evidence to suggest there is. Constructing smaller devices may increase performance, reduce undesirable heating effects, lower power consumption, decrease material wastage, increase storage capacity for a given volume, and improve overall efficiency. With these huge incentives to continually miniaturise products, the manufacture of specific technologies – such as computers - has started to approach the nanoscale (see figure 1.1). At the nanoscale new exciting properties emerge that are not observed at the macroscale. These properties may be extremely beneficial for certain applications. With respect to computing, this may permit the fabrication of extremely high speed circuits with increased processing power and storage space. However the advantages provided by the nanoscale are not limited to the field of computing. For example, materials such as carbon nanotubes, if arranged properly, have greater than 100 times the tensile strength of high-carbon steel[7]. This could completely revolutionise the entire mechanical engineering field. It should be noted however that it is not a simple matter to obtain benefits such as these; huge amounts of time and resources are required to realise the potential of the nanoscale.

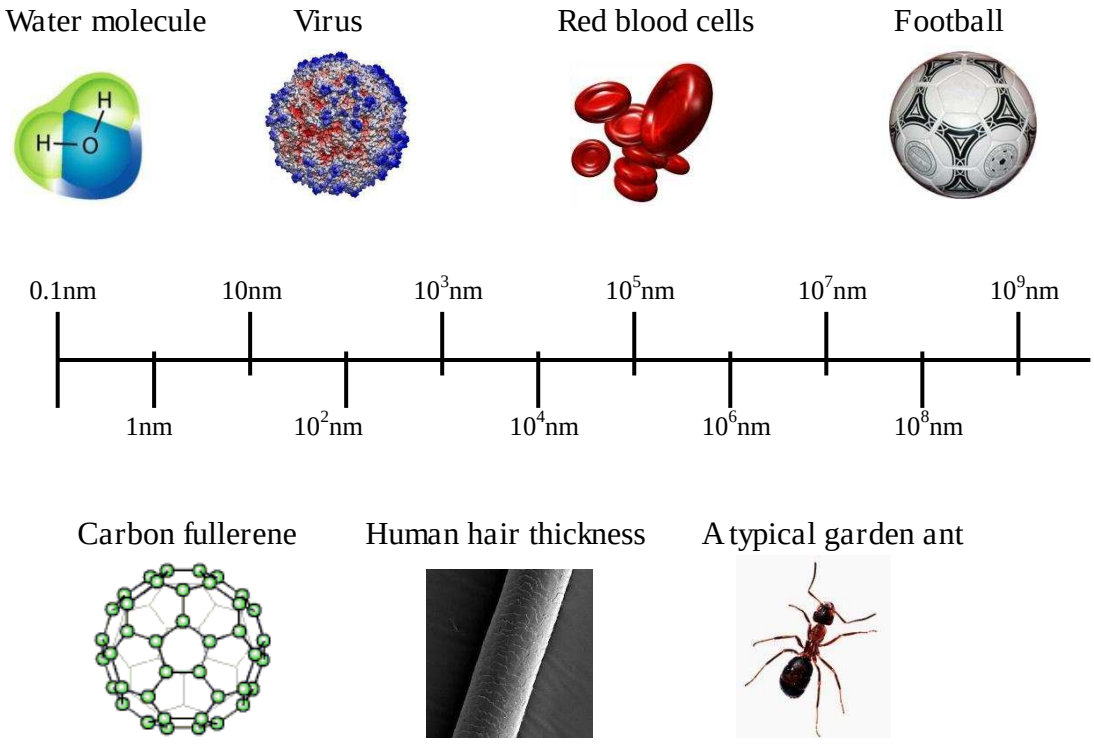

Figure 1.1: Relative sizes of various objects, illustrating the scale of the nanometre. A FIFA regulation football is roughly 300,000,000 times larger than a Buckminster fullerene (which is ~ 1nm).

When investigating science at the length scale of the nanometre the terms nanoscience and nanotechnology are relevant and have become widely adopted. However there is not a precise unified definition of the meaning of these two terms. The Oxford dictionary of physics defines nanotechnology as "The development and use of devices that have a size of only a few nanometres", and the Royal Society and Royal Academy of Engineering define nanoscience as "the study of phenomena and the manipulation of materials at atomic, molecular and macromolecular scales". It is broadly understood that nanoscience is the investigation and understanding of the properties of matter at the nanoscale; the use of knowledge gained from nanoscience, enabling technological applications, is termed nanotechnology. Therefore, given this broad definition, nanoscience and nanotechnology are highly multidisciplinary fields. Supramolecular chemistry, physics, mechanical engineering, materials science, biological engineering and pharmacy (to name just a few) are all encompassed within the nanoscience umbrella.

1.1.1. Nanoscience: A Brief History

The phrase "nanotechnology" was coined by Norio Taniguchi in the 1974 paper "On the basic concept of Nano-Technology"[8]. Although the phrase originated from this publication, aspects of nanoscience and nanotechnology actually pre-date it. In fact it may be argued there was no definitive beginning to the study of nanoscience; even as far back as 1912 principles of nanoscience were being investigated, for example through the work of W. L and W. H Bragg's on the determination the atomic arrangement of crystals by the diffraction of light. However, there was a distinctive and at the time highly original recognition of the potential of nanoscience which was articulated in the renowned "There's plenty of room at the bottom" lecture, presented by Richard Feynman at an American Physical Society meeting at Caltech, on December 29, 1959. Feynman spoke of a future where we have the ability to manipulate single atoms and molecules into ordered structures, enabling the fabrication of complex machines and devices at the nanoscale. He set two challenges to further research in the field: to build a nanoscale motor and to write words at a 1/25,000 of the scale used in this thesis - both of which have since been achieved[9]. Feynman introduced new concepts, a new way of thinking and provided inspiration for people to become

involved in nanoscience. It is therefore no surprise that many people regard this lecture as the conceptual origin of nanoscience.

Another significant development in the history of nanoscience was the 1991 publication "Nanosystems, Molecular Machinery Manufacturing and Computation" by K. E. Drexler. This publication had a great influence on the perception of nanoscience on journalists and, as a consequence, the general public. Furthermore, it brought nanoscience to the attention of the public for the first time introducing a radical new way of thinking, using rigid nanoscale gears, levers and other mechanical devices to self-assemble basic molecules into complex structures. According to Drexler this technology could revolutionise the science through the use of nanoscale self-assemblers able to create practically any structure from its component materials. However, this promising outcome was countered by a bleak vision of self-replicating nanobots. "Grey goo" – a phrase that became very popular with the press - refers to the predicted end of the world brought about by self-replicating nanobots that reduce all matter on earth into "grey goo".

It is worth noting that many of Drexler's visions remain highly speculative and appear to violate known physical principles. It is not known if the nanoscale machines he envisioned may be fabricated; more specifically, there are questions with regards to scaling factors, such as the dominance of friction at the nanoscale, and the emergence of phenomena that are not significant at the macroscale - such as the Casmir force. As these issues remain unclarified, it cannot be stated whether Drexler's visions are viable or not. But there is evidence to suggest that within the laws of nature there is the potential to create complex structure from basic components - we only need to look at biology. Biology, which uses solution based chemistry and soft materials, is a complete contrast to the mechanisms proposed by Drexler but the information contained within DNA permits a single cell to self-assemble into a massively complex human being. Whether this capability can be emulated by the use of science is not known, but it is apparent that nanoscience has huge potential.

1.1.2. Introduction to STM and TEM

With regards to this thesis there are two technologies that are of specific relevance - both of which have made a significant contribution to nanoscience. They are briefly introduced in the following paragraphs.

One of the most influential advances in the field of nanoscience was the development of the scanning tunneling microscope (STM) in 1981 by Bining, Rohrer and Gerber[10]. This microscope used a similar principle to the profilometer[14]; by translating an atomically sized conductive tip line by line over an area, hence providing information about surface topography. The STM has revolutionised study at the nanoscale, especially in the field of surface science[1]. In recognition of the enormous impact of the development of the first STM, Bining and Rohrer were awarded the Nobel Prize for Physics in 1986 – just 5 years after its discovery. The invention of the STM has led to other novel instruments such as the atomic force microscope (AFM) and the scanning capacitance microscope (SCM). These technologies are collectively known as Scanning Probe Microscopy (SPM) and their emergence has provided many exciting advances and discoveries.

Another very influential instrument, which has aided our knowledge of how matter behaves at the nanoscale, is the transmission electron microscope (TEM). This instrument, developed by Hillier et al. in 1938, emits electrons from a cathode, by thermionic or field emission. The electrons are then focused onto an extremely thin sample (~100 nm thick) using magnetic lenses. The TEM then constructs images based on the scattering and diffraction of electrons from the crystal structure of the sample. The instrument has been extremely influential in the fields of mechanical and biological sciences[11]. In contrast to STM, TEM provides an entirely different but complementary set of data.

1.2. Thesis Outline:

The previous chapter has provided some history and defined a few of the terms used in nanoscience. It has also given a brief introduction of the two technologies used throughout this thesis: STM and TEM. Chapter 2 goes on to explain the basic principles behind STM. Key formulas are derived to help gain a better idea of the mechanisms that occur in STM, aiding in the interpretation of STM images and data. A brief introduction to TEM, its history and previous applications are provided in chapter 3. The advantages of conducting in-situ TEM investigation are also highlighted, with special emphasis on in-situ STM applications.

In chapter 4, the design of the in-situ STM I developed at Nottingham University is presented. All decisions taken in the design stages are discussed and the basic mechanisms employed in the STM are explained. In addition, a description of the tests conducted to evaluate the performance of the in-situ STM is included. Information about the first application for the Nottingham built in-situ STM is presented in chapter 5; this chapter is primarily concerned with the study of the solid electrochemical process in silver sulphide (Ag_2S) crystals.

Chapter 2:

Scanning Tunneling Microscopy

The scanning tunnelling microscope was developed in 1981 by Binnig, Rohrer et al[12] for which they were awarded the Nobel Prize for physics in 1986. STM was the first technique capable of real space imaging with atomic resolution, and it rapidly became an essential tool in the field of nanoscience.

2.1. Electron Tunneling

The quantum mechanical effect known as tunneling underpins the acquisition of high-resolution images in STM (illustrated in the planar electrode model, figure 2.1). Tunneling of electrons occurs when two conducting surfaces are in close enough proximity that their surface electron wavefunctions significantly overlap[13]. Electrons are able to tunnel from one surface to the other, provided there is an unoccupied electron state with the same energy on the other surface. Classically this is impossible because the electron does not have enough energy to overcome the potential barrier

associated with the separation of the two conductors, but tunneling is an intrinsically quantum mechanical effect.

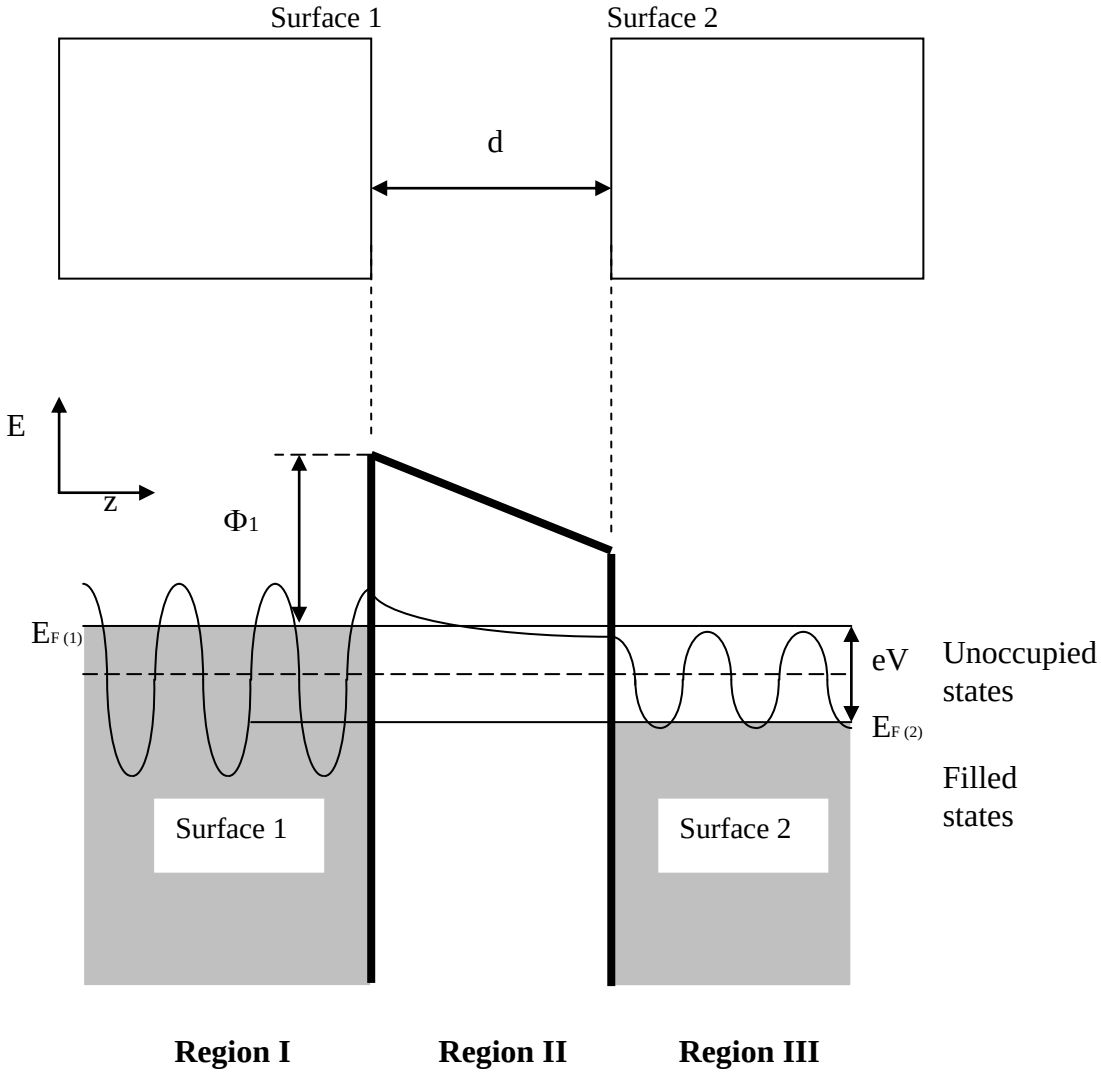

Figure 2.1: Diagram illustrating the energy distribution in a tunnelling junction, between two conducting surfaces in one dimension (x-direction), assuming a rectangular potential barrier. A potential difference of V is applied between surfaces 1 and 2. Only electron states with energies between $E_{F(1)}$ - eV and $E_{F(1)}$ can tunnel to unoccupied states to $E_{F(2)}$ to $E_{F(2)}$ + eV. These electrons do not have enough energy to *overcome the workfunction* Φ_1 but, due to electron wave-particle duality, are able to tunnel to surface 2.

The net charge flow from one surface to another is called the tunneling current. The form of the tunneling current is derived by the superposition of the overlapping electron wavefunctions. In region I, the electron wavepacket is contained within the bulk

material. Consequently, the wavefunction can be expressed as the superposition of two oscillating waves: one wave travelling in the positive x-direction and one in the negative x-direction (from the reflection of the positive x-directional wave by the potential barrier between regions I and II).

$$\Psi_I = Ae^{ikz} + Be^{-ikz} = e^{ikz} + Be^{-ikz} \quad \text{as A = 1} \qquad (2.1)$$

Where A and B are constants, $k = \sqrt{\frac{2mE}{\hbar^2}}$, E is the total energy of the electron and z is a spatial dimensional axis. In region II, the wavefunction can be represented by the superposition of two exponential functions.

$$\Psi_{II} = Ce^{iKz} + De^{-iKz} \qquad (2.2)$$

Where C and D are coefficients of the transmission and reflection of the potential barriers, $K = \sqrt{\frac{2m(V_0 - E)}{\hbar^2}}$, V_0 is the height of the potential barrier. In region III, the wavefunction is not a superposition of two oscillating waves as there is no potential barrier to the far right able to reflect back the incident wave. Thus, the wavefunction is simply a single term.

$$\Psi_{III} = Fe^{ikz} + Ge^{-ikz} = Fe^{-ikz} \qquad \text{as G = 0} \qquad (2.3)$$

Where F is the coefficient of transmission through the potential barrier between regions II and III. The coefficients B, C, D and F can be derived from boundary conditions and that the wavefunction, ψ, and its derivative, $\frac{d\psi}{dx}$, are continuous[14]. To acquire the transmission of the electron wavepacket through the potential barrier the transmission current density, j, needs to be considered, which is expressed in the form below.

$$j = \frac{\hbar}{2im}\left(\Psi^* \frac{d\Psi}{dz} - \frac{d\Psi^*}{dz}\Psi\right) \qquad (2.4)$$

The incident current (j_i) and transmission current (j_t) densities can be expressed as,

$$j_i = \frac{-i\hbar}{2m}, \qquad j_t = \frac{-i\hbar}{2m}\left|F\right|^2 \tag{2.5}$$

The total transmission coefficient T can be expressed as the ratio of the current density transmitted through region III to region I.

$$T = \frac{j_{III}}{j_I} = \left|F\right|^2 \tag{2.6}$$

T is dominated by the term e^{-2Kd} and is a continuous function of barrier width and height. Consequently the tunnel current can be expressed in the form below[14].

$$I \propto e^{-2Kd} \tag{2.7}$$

Where I is the tunnelling current, d is the separation between the two surfaces and $K = \sqrt{\frac{2m\phi}{\hbar^2}}$, where ϕ is the workfunction. Equation 2.7 illustrates that the tunnelling current (I) is proportional to the exponential of the separation of the two surfaces (d). Assuming a workfunction of a few eV, an increase of ~2-5 Å in the separation between the two surfaces can produce a ~ three orders of magnitude decrease in the tunnelling current. It is the exponential dependence of the tunneling current on the separation of the surfaces that gives STM such good sensitivity in the z-direction.

Figure 2.1 shows the energy diagram for a tunnelling junction using the planar electrode model; a model that does not entirely represent the true nature of STM. In particular, STM uses one tip and a conducting surface instead of two planar electrodes. A tip is used in order to localise the tunnelling electrons to a smaller volume; the benefits of this will be discussed later in this thesis. To acquire a STM image, the tip is translated line by line over an area of the sample surface; the tunnelling current is monitored at each point in each line.

2.2. STM Imaging: Modes of Operation

In STM there are two modes of operation with which to scan a sample and produce an image: constant current mode (CCM) and constant height mode (CHM). In CCM (see figure 2.2a), the tip is translated in the x-direction (using piezoelectric transducers, section 2.5); if, due to the features on the sample surface, the tip-sample distance changes (i.e. d changes - equation 2.7) the magnitude of the tunnelling current will also change. In order to keep the tunnelling current at a constant magnitude a digital feedback loop, which adjusts the height of the tip at each measurement point, is employed. For example, if the tip translation in x results in a reduction of d, the tunnelling current will increase. The feedback mechanism will detect this increase and adjust the voltage applied to the piezoelectric transducers, resulting in a retraction of the tip from the sample surface. In this way the tip follows the contour of the sample topography (neglecting electronic contributions). The magnitudes of the voltages applied to the piezoelectric transducers provide the contrast in the STM image.

Figure 2.2:

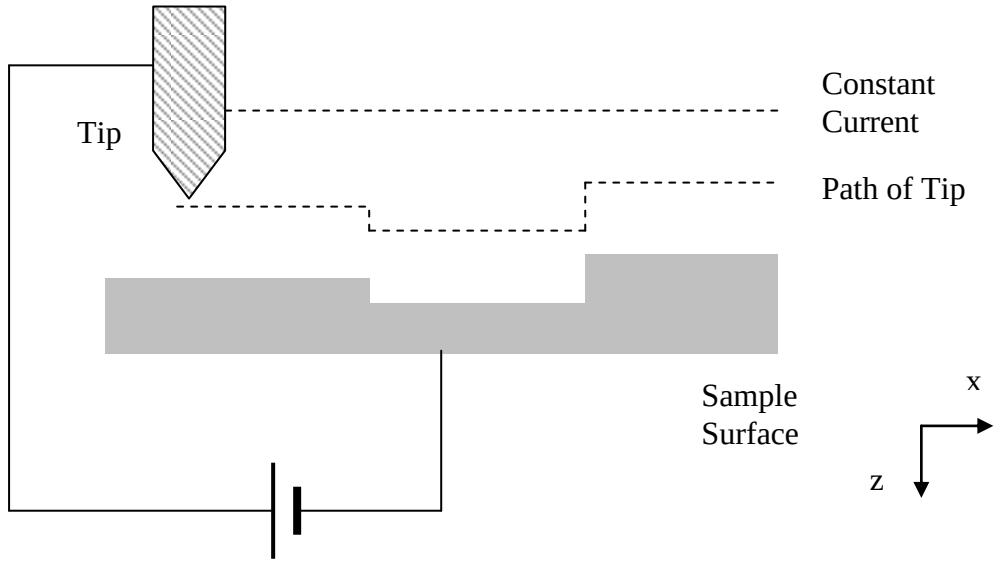

a) In constant current mode (CCM), as the STM tip is translated across the sample a feedback loop adjusts the height of the tip at each measurement point. Thus the tip follows a contour of the sample topography, neglecting local surface electronic inhomogeneties.

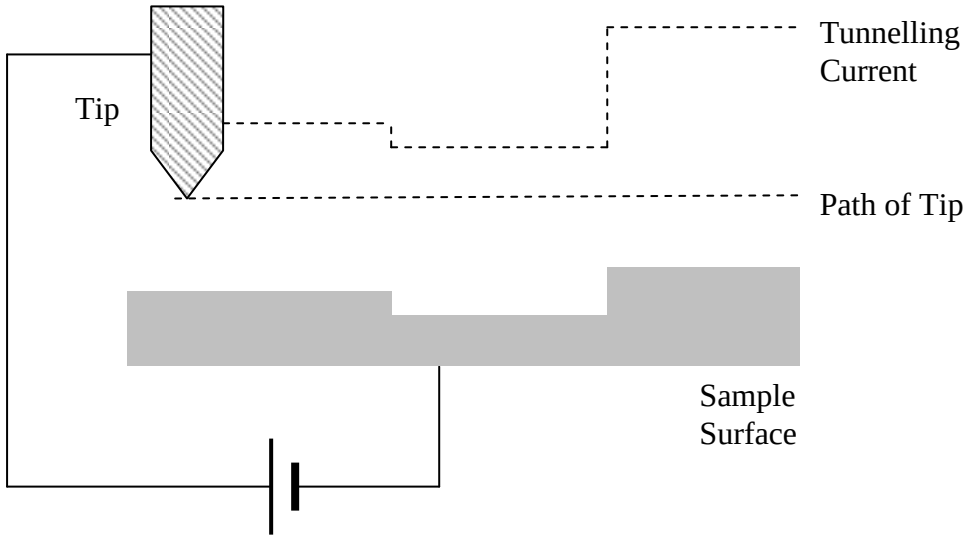

b) In constant height mode (CHM) the STM tip is translated across a horizontal plane above the sample surface. The variations in the tunnelling current reflect the topography and local electronic properties of the surface.

In CHM (figure 2.2b), the mechanism is slightly different; the STM tip is translated in a horizontal plane and as the tip-surface separation varies, due to changes in surface topography and local surface electronic properties, the tunnelling current increases or decreases respectively (equation 2.7). In CHM the variation of the tunnelling current provides the contrast in the image.

The CCM and CHM techniques both have their own merits and limitations. CHM provides faster information acquisition, as it does not have a time limiting feedback mechanism, but as a consequence is prone to crashing the tip into the sample. CCM however, is the most widely used method of operation because the feedback mechanism permits large scans to be acquired on uneven sample surfaces without tip crashes; for this reason CCM is used through the entirety of this thesis.

2.3. Interpretation of STM Images

Equation 2.7 states that the log of the tunnelling current is proportional to the distance between the two conducting surfaces. In CCM, the feedback mechanism maintains a constant current by varying the tip/sample distance (via piezoelectric transducers). Therefore, assuming a surface with a constant workfunction, a STM image represents the topography of the surface. However the simple rectangular potential model

described above does have limitations when describing the tunnelling current. A closer approximation was formulated by Tersoff and Hamann[15] using principles formulated Bardeen[13]. A more general expression for the tunneling current is

$$I = \frac{2\pi e}{\hbar} \sum f(\varepsilon_\mu)[1 - f(\varepsilon_\nu + eV)]\left|M_{\mu\nu}\right|^2 \delta(\varepsilon_\mu - \varepsilon_\nu) \qquad (2.8)$$

Where e is the electron charge, ε_μ is energy of state μ, $f(\varepsilon_\mu)$ is the Fermi-Dirac distribution function, $M_{\mu\nu}$ is the matrix transfer element between states μ and v, and δ is the delta function, which ensures conservation of energy between initial and final states. Equation 2.8 states that for tunnelling to occur there must be a finite probability that an electron is in a specific state $f(\varepsilon_\mu)$, and that it can only tunnel into an unoccupied state$[1-f(\varepsilon v+eV)]$. The matrix element ($\left|M_{\mu\nu}\right|^2$) contains information regarding the probabilities of transfer between specific electron state μ and v. It is worth noting however, that certain approximations have been applied; only elastic tunnelling is considered, i.e. the initial electron state (μ) has to have the same energy as the final state (v). Equation 2.8 can be simplified further[15] in the limit of small voltage and temperature, giving

$$I = \frac{2\pi}{\hbar} e^2 V \sum_{\mu,\nu} \left|M_{\mu\nu}\right|^2 \delta(\varepsilon_\nu - \varepsilon_F)\delta(\varepsilon_\mu - \varepsilon_F) \qquad (2.9)$$

Where V is the applied bias and ε_F is the Fermi energy. Further simplification of equation 2.9 can be achieved by considering the case where the tip is replaced with a point probe (i.e. a tip of zero radius of curvature). If the tip is considered a point probe the electron wavefunctions are completely localised, therefore the matrix element is proportional to the probability of finding an electron at the tip apex (i.e. $\left|\psi\right|^2$).

$$I \alpha \sum_\nu \left|\psi_\nu(\vec{r}_0)\right|^2 \delta(\varepsilon_\nu - \varepsilon_F) \qquad (2.10)$$

Where ψ_v is the electron wavefunction and r_0 is the centre position of the spherical tip. This method is known as the transfer Hamiltonian (TM) approach[13], where the tunnelling current is expressed in terms of the unperturbed wavefunctions of the tip and sample. The quantity on the right hand side of the equation is the surface electron local

density of states (LDOS) at the Fermi level. Therefore, a STM image is said to represent a contour of constant LDOS at the Fermi level. The TM approach is not an exact description of electron tunnelling but relates it to a simple, physical quantity (the LDOS) for easy visualisation. Noguera et al formulated a very accurate calculation of the tunnelling current but it is more abstract in nature[16]; depending on a quantity which is related to the LDOS but not proportional to it.

An STM image is not only dependant on the LDOS of the sample, but also the LDOS of the tip. To produce a realistic model of STM, the tip must have a finite size. Modelling a tip with finite size will effectively convolve the sample LDOS data with the tip LDOS data; this has the effect of blurring the image produced and limiting the lateral resolution of the STM. To account for the extent of this blurring, the exact geometry of the tip must be known. This is extremely difficult to obtain and can change in the process of imaging.

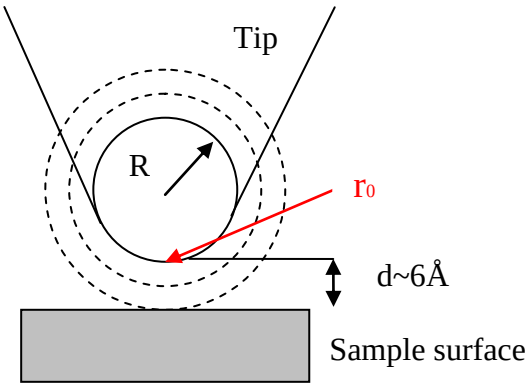

Figure 2.3: Diagram showing the spherical symmetric nature of the tip used in Tersoff *and Hamman's model for inter*preting STM data.

To overcome this problem, Tersoff and Hamman modelled the tip as a spherically symmetric potential[15] - an s-wave with a radius of curvature R (see figure 2.3). This approximation provides some information with regards to the effect of the tip on the STM data obtained. However without actually imaging the tip geometry, the radius of curvature can only be estimated. Interestingly, a solution to this problem may be found by using in-situ STM in TEM (discussed later in this report), which will allow the STM tip to be viewed whilst simultaneously conducting STM experiments.

2.4. Non-Imaging STM Techniques

2.4.1. Scanning Tunnelling Spectroscopy

As STM acquires data related to the LDOS, it provides the opportunity to acquire spectroscopic information about a sample. Scanning tunnelling spectroscopy (STS) is a technique employed to obtain information about the local electronic surface states by observing the variation of the tunnelling current with respect to the applied tip/sample bias. It uses the principle that the derivative of the tunnelling current, with respect to the bias, can be expressed in the form below.

$$\frac{dI}{dV} \propto \rho_s(E_F - eV) \qquad (2.11)$$

Where ρ_s is the LDOS of the sample. Hamers et al. devised an experiment, using current-imaging tunneling spectroscopy (CITS)[17], to obtain the LDOS of a sample. In this experiment the quantity dI/dV was measured as a function of the applied bias, which was varied from -2.5 V to + 2.5 V. The electronic feedback mechanism was disabled, thus the tip was stationary throughout the experiment, i.e. tip-sample distance was kept constant. The measured value of dI/dV could be used to estimate the surface electron LDOS of the sample using equation 2.11.

2.4.2. STM Manipulation

STM can also be used to manipulate individual atoms, molecules and nano-objects. One of the most famous images in nanoscience (shown in figure 2.4) is the manipulation of Xe atoms on a Ni surface, conducted by Eigler and Schweizer[18], spelling out the name "IBM". Manipulation essentially consists of moving individual atoms, molecules or nano-objects on a surface without moving any surrounding material. This can be achieved in a number of ways, including lateral manipulation and vertical manipulation.

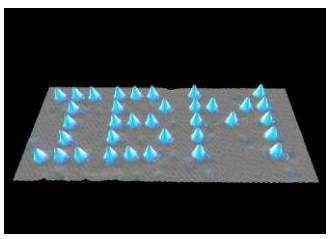

Figure 2.4: STM image of Xe atoms, on a Ni substrate, arranged by lateral molecular manipulation to spell IBM.

The first step in the lateral manipulation process (figure 2.5) involves acquiring a STM image and choosing a suitable object atom or molecule to manipulate. The STM tip is then positioned near the object of interest and is moved towards the sample surface (1), by increasing the tunnelling current setpoint or reducing the tip-sample bias (operating in CCM). Once the tip is in position, it is translated across the sample surface (2) with the STM feedback mechanism still in operation. The close proximity of the tip to the object results in lateral forces acting between them; the object is shifted in the direction of the tip movement. According to Rieder et al[19] three main lateral manipulation modes have been distinguished: "pulling", "pushing" and "sliding". "Pulling" consists of the tip interacting with the object via attractive Van der Waals forces, the tip effectively pulling the object across the sample surface. "Pushing" involves repulsive forces, i.e. the repulsive regime of the Lennard-Jones potential (figure 2.6), of the tip and object; forcing the object in the tip's direction of motion. Finally "sliding" consists of trapping the object under the tip and smoothly translating it across the surface. Once the object has been moved the tip is retracted, by adjusting the bias and current values (3), and then translated back to its original position (4). This was the technique employed to arrange the Xe atoms in figure 2.4.

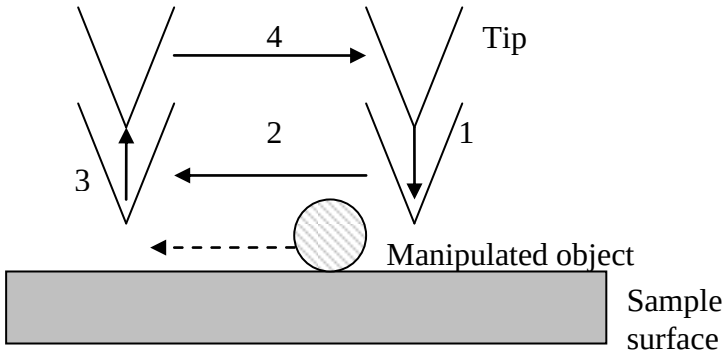

Figure 2.5: Diagram illustrating the process employed to laterally manipulate nano-objects

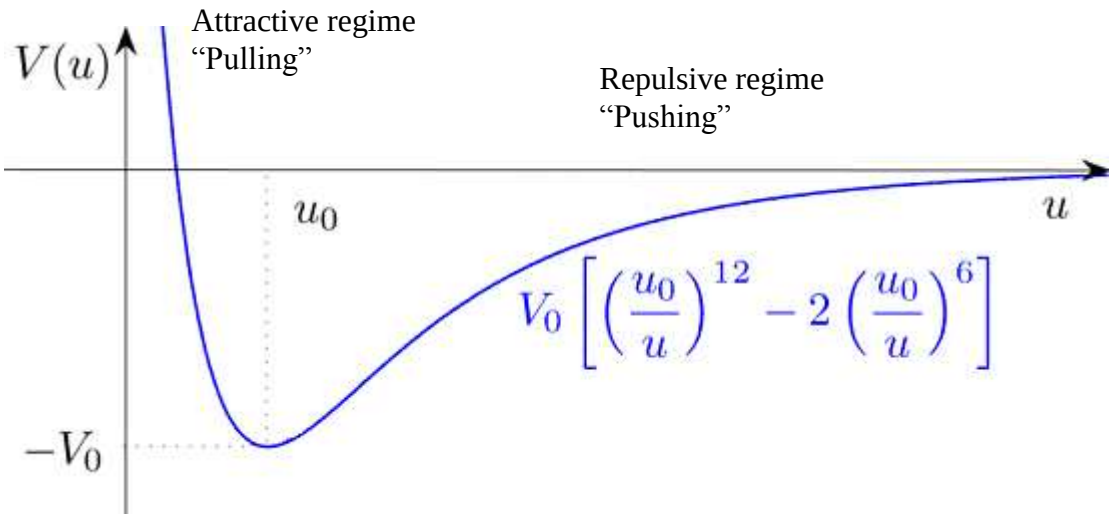

Figure 2.6: Lenard-Jones potential

Vertical manipulation (figure 2.7) involves positioning the STM tip directly above the object to be manipulated. The object can then be “picked up” by the STM tip using two methods. At approximately a 6Å tip-object separation, an electric field can be applied between the tip and object. The applied electric field lowers the potential barrier between the object and the tip, enabling transfer of the object to the tip. This method uses the double potential well model[20] (figure 2.7b). The other method used to overcome the potential barrier is to simply crash the tip directly into the object. Once the object is attached to the tip it can be positioned anywhere (using the piezoelectric transducers on the tip). By applying a reverse polarity bias, it becomes energetically favourable for the object to attach back to the surface.

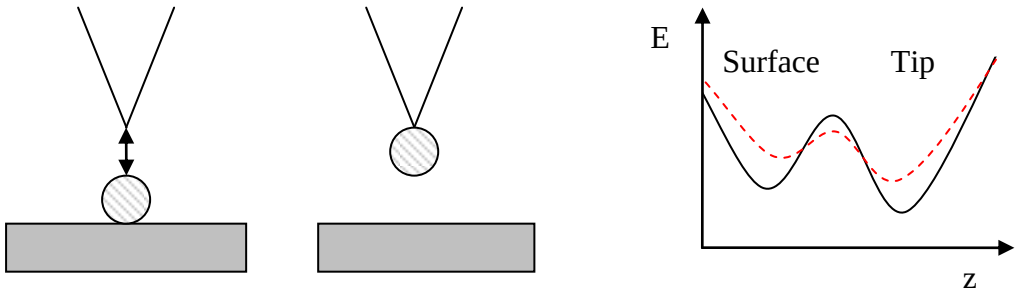

Figure 2.7: a) Diagram illustrating the process used to vertically manipulate atoms/molecules/nano-objects. b) The double potential well model (the dashed line is the potential variation after an applied electric field between tip and sample).

There is much that is unknown about the mechanisms that govern STM manipulation. In-situ observation of STM manipulation events may help to provide more information.

2.5. Positional Control for the STM

2.5.1 The piezoelectric effect

For a STM to be able to scan a surface and resolve individual atoms there must be a method of achieving controlled tip motions to sub angstrom precision. Using the principles of the inverse piezoelectric effect, this precision is achievable. Piezoelectricity arises from the crystal structure of the material, with 20 crystal classes exhibiting piezoelectricity [21]. For a crystal to be piezoelectric, the positive and negative charges located inside the crystal need to be spatially separated, creating an electric dipole - the crystal is still electrically neutral due to the symmetric distribution of these charges. The electric dipoles form domains that will align when exposed to an external electric field, which in turn will cause the mechanical deformation of the crystal. The electric displacement of the piezoelectric crystal is linearly dependant on the applied voltage. This allows the extension of these piezoelectric crystals to be controlled to sub nanometer precision. The inverse piezoelectric effect is exploited for coarse and fine positional mechanisms in the STM as explained in the following sections.

2.5.2 The principles of inertial sliding mechanisms

The placement of the STM tip close to the sample, down to a separation of around 100nm, is known as coarse positioning. Two main methods are usually employed: mechanical adjustment and inertial sliding mechanisms – also known as “slip-stick” motors. Mechanical adjustment employ gears to attain very small and controllable movements often based on differential screws. However, inertial sliders are the most commonly used method of coarse positioning since their introduction by Pohl[22]. The inertial sliders investigated in the following section are used within the Nottingham

developed in-situ STM; they use a slightly different mechanism to standard inertial sliders but still use the same fundamental principles.

The in-situ STM inertial sliders consist of a weight that is attached to a piezoelectric crystal, which is in turn attached to a material of low coefficient of static and kinetic friction (see figure 4.4). The low friction material is held in position using a clamping mechanism. When a potential difference is rapidly ramped between the inner and outer electrodes of the piezoelectric tube, the piezoelectric crystal expands (see figure 4.4b). The force produced by this expansion will accelerate the low coefficient material. If equation 2.12 is satisfied, then the rod will "slip" past the clamping mechanism, resulting in movement of the inertial sliding mechanism. The purpose of the weight is to provide enough inertia to drive the rod in the desired direction.

$$a_l > \frac{\mu_s N}{m_l} \qquad (2.12)$$

Where μ_s is the coefficient of static friction, N is the normal force of the clamping mechanism on the low friction material and m_l is the mass of the low friction material. Once the piezoelectric material has achieved maximum extension, the potential difference between the electrodes is gradually reduced, so that the acceleration of the rod is

$$a_l < \frac{\mu_s N}{m_l} \qquad (2.13)$$

The piezoelectric crystal will contract in size, and because of the reduced acceleration at which the piezo contracts, the low friction material will remain clamped by the clamping mechanism. Net motion is achieved (see figure 4.4c).

Figure 4.4: Inertial sliding slip-stick drives

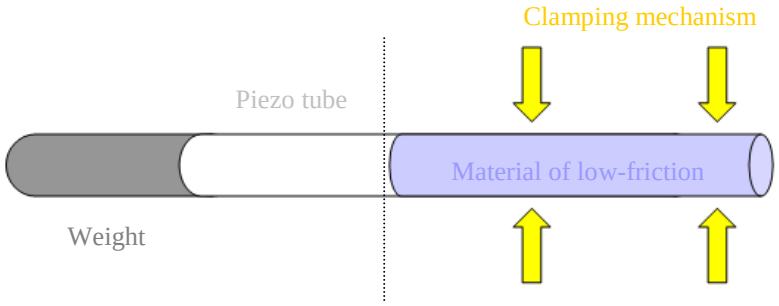

a) Schematic of the inertial sliding drives employed by the Nottingham developed in-situ STM

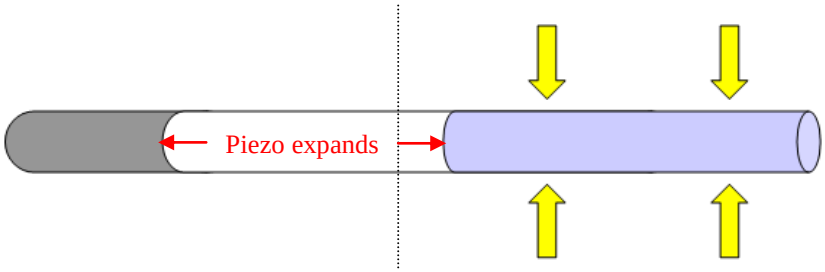

b) By quickly applying an exponentially ramped potential difference between the outer and inner piezo electrodes, the low-friction material will slide past the clamping mechanism

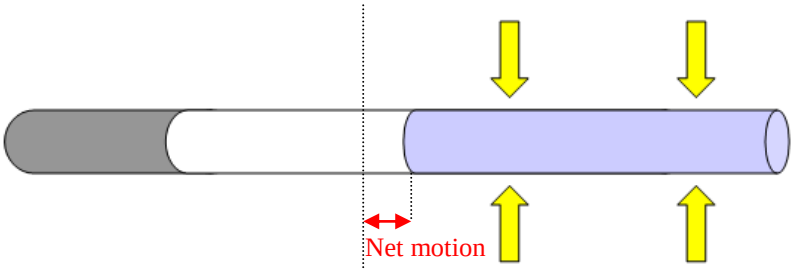

c) Slowly reducing the potential difference between the outer and inner electrodes will make the low friction material stick to the clamping mechanism. A net movement is achieved.

2.5.3 Fine positional mechanism

While slip-stick motion is adequate for achieving coarse position, it is not sufficiently precise at small scales (i.e. nm range); this is predominantly due to the unpredictable motion of the low friction material as it slides between the clamping mechanisms. For more precise positioning, i.e. for scanning the STM tip, a piezoelectric tube is used (figure 4.5).

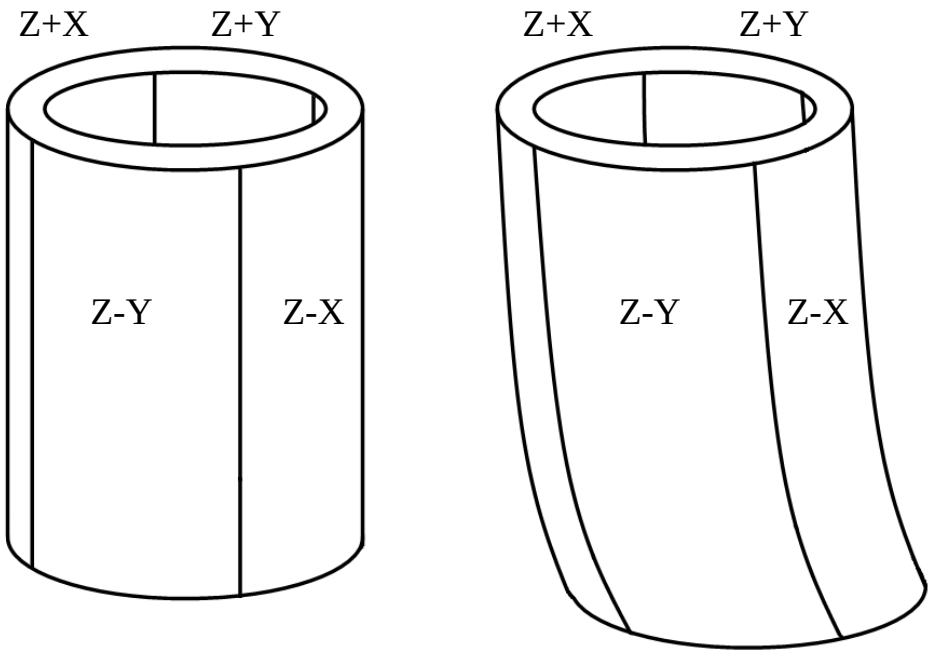

Figure 4.5: a) Schematic of a piezoelectric tube showing the four outer piezoelectric electrodes: Z+X, Z-X, Z+Y and Z-Y. b) Application of a voltage to the Z-X and Z+X electrodes causing distortion of the tube in the x-direction.

A piezoelectric tube is essentially a cylinder made of a piezoelectric material, usually lead zirconate titanate (PZT). This cylinder has five electrodes: one inner electrode and four outer electrodes. Application of a potential difference between these electrodes allows controlled motion in three dimensions. To achieve z-directional motion, a potential difference is applied between all four outer electrodes and the inner electrode. For x-directional motion, a potential difference is applied between the Z+X and Z–X electrodes with respect to the inner electrode; the tube then distorts and motion in the x-direction is achieved (figure 4.5b). Similarly, to achieve motion in the y-direction a potential difference is applied to Z+Y and Z-Y electrodes with respect to the inner electrode. The use of piezoelectric crystals means there is no dependence on unpredictable frictional motions associated with inertial sliders. As such, very precise and controllable motions can be achieved.

2.6. Vacuum STM

Many STM applications are conducted in ultra high vacuum conditions (UHV ~10^{-9} Pa). This is to ensure that contamination of the tip and sample, from physisorption/chemisorption of molecules in the air, is kept to a minimum. To achieve and maintain UHV conditions, a STM may use any combination of the three major pumping techniques: positive displacement, momentum transfer and entrapment. To improve the vacuum further, a STM chamber can possess an in-situ heater designed to evaporate contaminants within the chamber in a process known as "baking". In addition, a UHV STM is usually encased within a stainless steel chamber. Stainless steel is an effective material to maintain vacuum conditions as it is difficult for even small molecules to penetrate the material's surface. A comprehensive guide to vacuum STM can be found here[23]; this thesis however is concerned only with achieving high vacuum conditions (HV~10^{-5} Pa) - present in the JOEL 2010F TEM. Given these less strict conditions the main concern in maintaining HV is to ensure that contaminants are not introduced into the TEM column; therefore everything was cleaned using the chemical solvents acetone, methanol and isopropanol before insertion into the TEM. In addition, it is vital that all materials inserted into the TEM have a low vapour pressure to prevent out-gassing, which will degrade vacuum conditions.

2.7. Sample and tip preparation

As mentioned previously, it is beneficial to have a sharp tip to perform STM experiments. There are two main methods of producing sharp tips in STM: mechanical cutting and electrochemical etching. Mechanical cutting simply consists of cutting the wire to be used as a tip at an angle to form an acute point. Electrochemical etching is a more complicated method and the process is specific to the tip material. To produce tungsten STM tips, tungsten wire (usually around 250 μm diameter) is placed into an etchant - NaOH[24]. The wire is submerged and an electrical potential difference is applied between the etchant and the tip. This potential difference initiates the electrochemical process, where the NaOH splits into ions (Na^+ and OH^-) that travel to the corresponding electrodes. At the point on the wire that touches the etchant meniscus there is increased activity; here the wire wears away very rapidly and this eventually causes the wire to break. As the wire breaks, the bottom end of the wire drops (via

gravity) leaving a sharp tip. Figure 2.8 shows a SEM image of a tungsten tip that I prepared (radius of curvature of ~ 100nm).

Tungsten is generally the material of choice for a vacuum STM tip, as it is relatively simple to produce tips of small radius of curvature using the electrochemical method; in this thesis all in-situ STM tips were made of tungsten. However, in air tungsten has a large oxide layer that hinders tunneling. Therefore, when performing STM in air, platinum iridium tips were fabricated - using the mechanical cutting method.

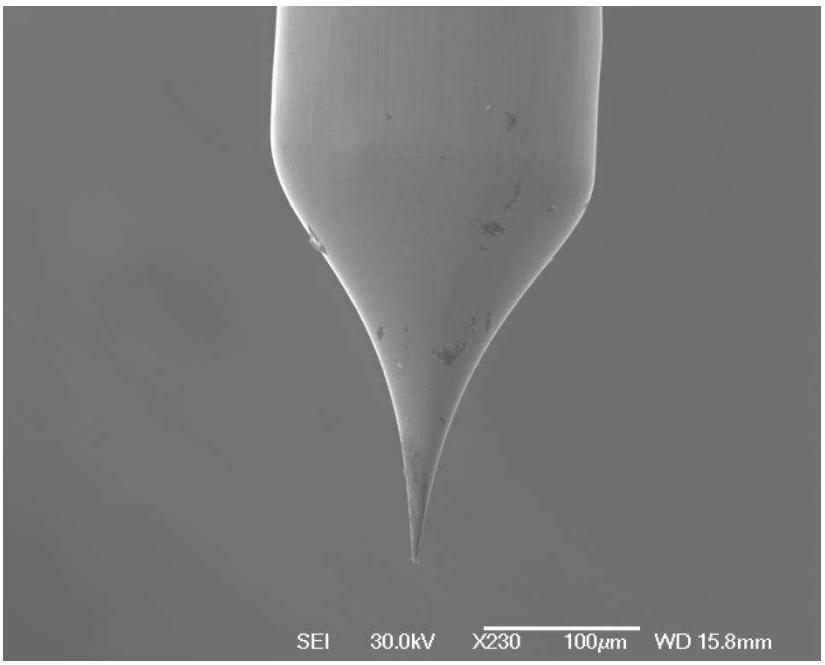

Figure 2.8: SEM image of a tungsten tip etched with NaOH

Chapter 3:

Transmission Electron Microscopy

The first electron microscope was developed by Albert Prebus and James Hillier at the University of Toronto in 1938. Before then only optical microscopy allowed observation the microscopic world. However, there are fundamental limitations of the resolution of optical microscopes. These limitations arise from the Rayleigh criterion (equation 3.1).

$$\delta = \frac{0.61\lambda}{\mu \sin \vartheta} \qquad (3.1)$$

Where δ is the resolution, μ is the refractive index of the medium, θ is the semi angle of collection of the magnifying lens, λ is the wavelength of the electromagnetic radiation. From equation 3.1 it can be ascertained that the major inhibiting factor of resolving smaller objects is the wavelengths of the incident particles. Visible light has a wavelength of ~ 400-700nm, giving a theoretical maximum resolution of 244nm (taking $\theta = \pi/2$ and μ= 1). At this wavelength it is not possible to resolve individual

molecules or atoms. However, this resolution limit can be overcome by using waves of higher frequency in the electromagnetic spectrum, such as UV rays or X-rays, but difficulties arise. UV rays are too readily absorbed by materials and X-rays are extremely difficult to focus and do not interact with matter readily enough. However, using the principle that all matter has a wave-particle nature, the De Broglie equation (equation 3.2), a solution can be found.

$$\lambda = \frac{h}{\rho} \qquad (3.2)$$

Where h is Planck's constant, and ρ is the particle momentum. Thus if electrons, for example, are accelerated to high velocities they will have a much smaller wavelength than visible light (a 200keV TEM produces electrons of wavelength ~ 0.003nm). Electrons can provide far greater resolution than ordinary light and are able to resolve individual atoms.

3.1. Basic Principles of TEM

In TEM electrons are fired at a sample and through observation of their interactions an image can be formed (figure 3.1). The electrons are produced by an electron gun, of which there are two types: a thermionic gun or a field emission gun (FEG). In a thermionic gun, a metal filament (usually tungsten) is heated and electrons are thermally emitted. In a FEG a very strong electric field is used to extract electrons directly from the filament. The purpose of an electron gun is to produce a fine beam of electrons of uniform energy and guide the beam towards the TEM optical axis. The whole of the TEM chamber is under high vacuum ($\sim 2\times10^{-5}$ Pa) to prevent the electrons colliding with particles present in air and to maintain the uniformity of the electron beam. After the electrons leave the electron gun they reach the condenser lenses, which are large magnetic coils used to focus the electrons into a thin, coherent beam and direct them towards the sample. These magnetic lenses use the principle that moving charges are subject to forces in a magnetic field. Therefore, charged particles such as electrons can be focused onto a specific area.

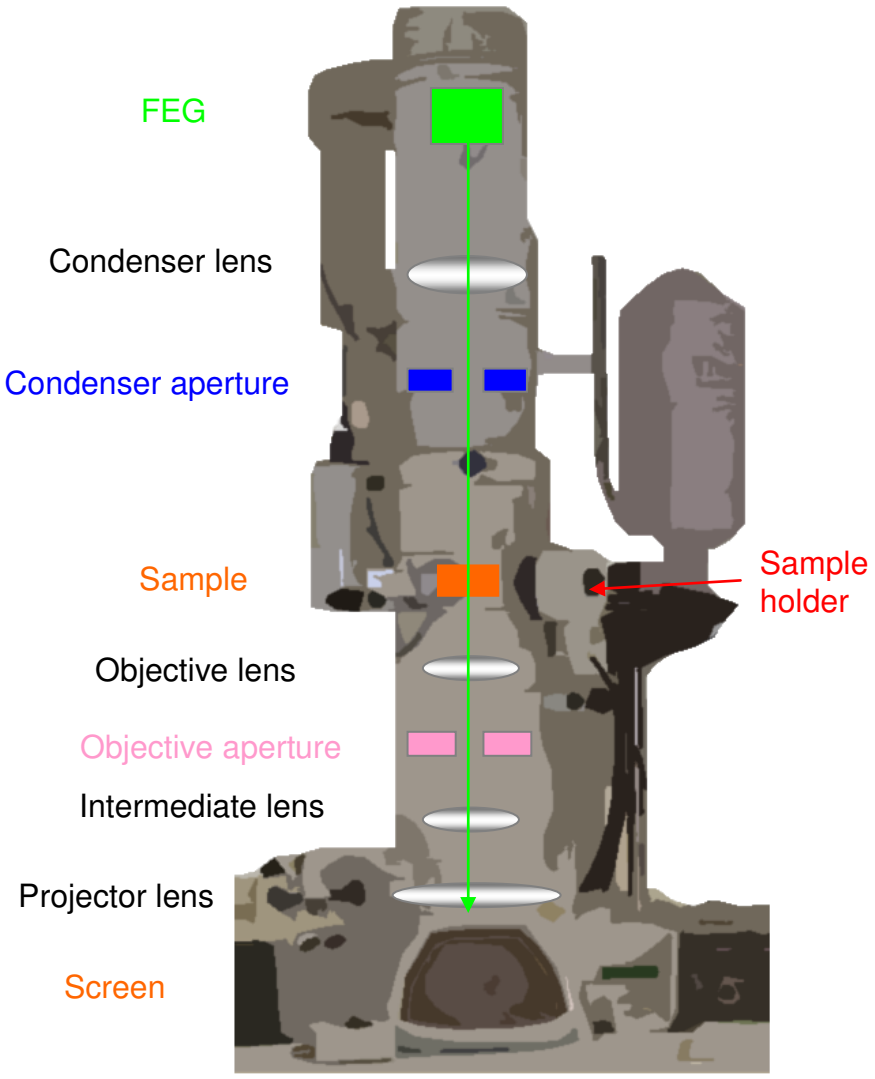

Figure 3.1: Diagram illustrating the basic structure and operation of a TEM.

The condenser aperture is located underneath the condenser lens; its role is to remove any electrons that deviate by a wide angle from the optic axis. Thus, via the condenser lenses and aperture, a narrow beam of electrons is focused onto the sample. Figure 3.2 shows the ways in which the incident electrons interact with the sample.

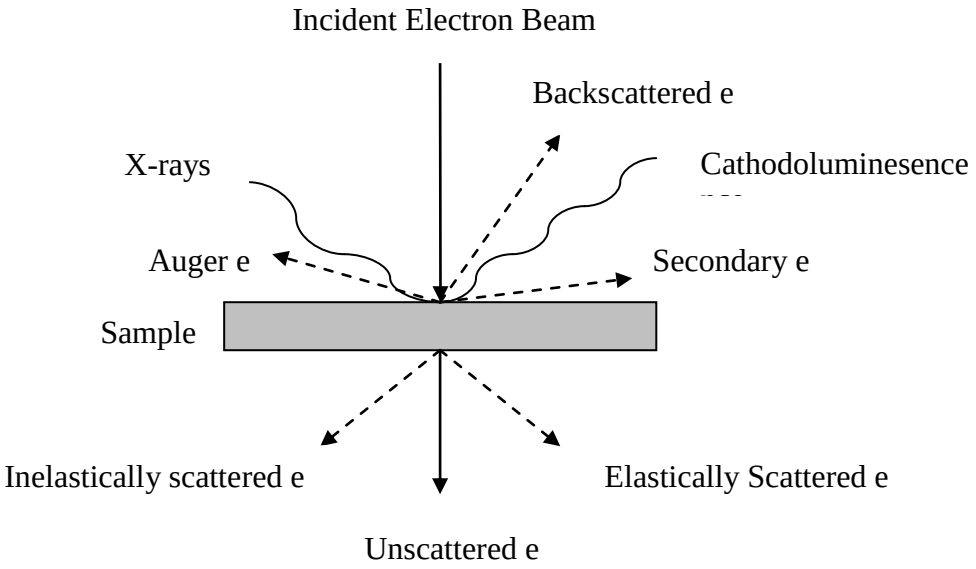

Figure 3.2: Diagram illustrating the possible interactions of electrons with matter. Backscattered electrons arise from incident electrons that interact with the positively *charged nucleus of an atom. When an incident electron "knocks out" an inner shell* electron - creating a hole - an x-ray or Auger electron is released when an outer shell electron fills this hole. Elastically scattered electrons usually consist of electrons diffracted by the lattice of the sample.

Elastically scattered electrons and unscattered electrons provide the contrast in TEM images, known as diffraction contrast. The transmission of unscattered and elastically scattered electrons must be maximised to improve the TEM image contrast. To achieve this, the sample thickness has to be very small (~ a few 100 nm) and should be no greater than the mean free path of the electrons. This is to improve the likelihood that only one scattering event takes place; meaning that diffracted electrons are not re-scattered, which would lower contrast in the image. The transmitted electrons then proceed towards the objective aperture; here electrons that have deviated from the optical axis are effectively blocked out. The position of this aperture is user controlled and can be positioned to select bright field and dark field operation. In bright field, the direct beam and unscattered electrons are employed to form an image, using diffraction contrast. In dark field, a diffracted beam of electrons are observed, this can provide information about imperfections and crystal geometry of a sample. Located after the objective aperture, are the intermediate and projection lenses. These lenses dramatically

enlarge the image and guide the electrons towards a charge coupled device (CCD) camera. This device is sensitive to incident electrons and produces the final TEM image. Figure 3.3 shows a photograph of the JEOL 2010F TEM. This is the TEM with which the in-situ STM is designed to be compatible.

Figure 3.3: Photograph of a TEM (model JOEL JEM 2010F).

3.2. Chemical Analysis in TEM

A TEM has a variety of different modes of operation. The JEOL 2010F TEM, used throughout this thesis, is capable of normal diffraction contrast imaging, in bright field and dark field, in addition to energy dispersive X-ray spectroscopy (EDX) and electron energy loss spectroscopy (EELS).

EDX is a tool used to analyse the chemical composition of a sample. It operates in a similar manner to standard TEM, i.e. an electron beam is guided towards the TEM optical axis. However, instead of producing an image, using unscattered and elastically scattered electrons (figure 3.2), EDX allows observation of the emitted X-ray properties. X-rays are produced when the passing electron beam ejects an inner shell electron in the sample - creating a hole. An electron from an outer shell will fill this

hole; hence lower the energy of the atom. An X-ray is emitted with energy equal to the difference between the electron energy levels in the transition, in order to conserve energy.

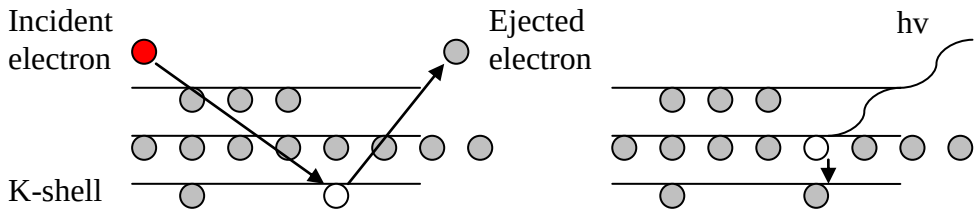

Figure 3.4: Diagram showing the process through which X-rays are emitted when an electron shell is bombarded by in incident electrons.

The emitted X-rays each have characteristic energies which are unique to each element. The X-rays are recorded and by observing the spectral lines produced in EDX the chemical composition of the sample can be obtained (see figure 5.3).

EELS, developed by James Hillier and RF Baker[25], is employed to acquire information regarding the atomic composition, chemical bonding, and surface electronic properties. In EELS, the sample in question is bombarded with a beam of electrons and the inelastically scattered electrons are observed, which have caused inner shell ionisation of the electrons in the sample. This results in a loss in energy of the incident electron and this loss can be used to identify the composition of the sample.

Both EDX and EELS are techniques that may be employed for in-situ STM experiments. The investigation of the atomic composition of the sample and tip is one potential advantage that EDX may bring to in-situ STM applications.

3.3. In-situ TEM applications

3.3.1. Basic Principles

The use of a non-standard TEM sample holder allows the investigation of a sample, using the TEM, but also permits additional data to be obtained simultaneously. These specialised sample holders come in a variety of types including SPM's[26], nano-indenters[27] and holders that provide tomography reconstructions[28]. To fit inside a TEM, between the pole pieces, the specialised holder is designed to exactly mimic the outer

dimensions of a standard TEM sample holder (figure 3.5), but has internal mechanisms that allow additional data to be gathered.

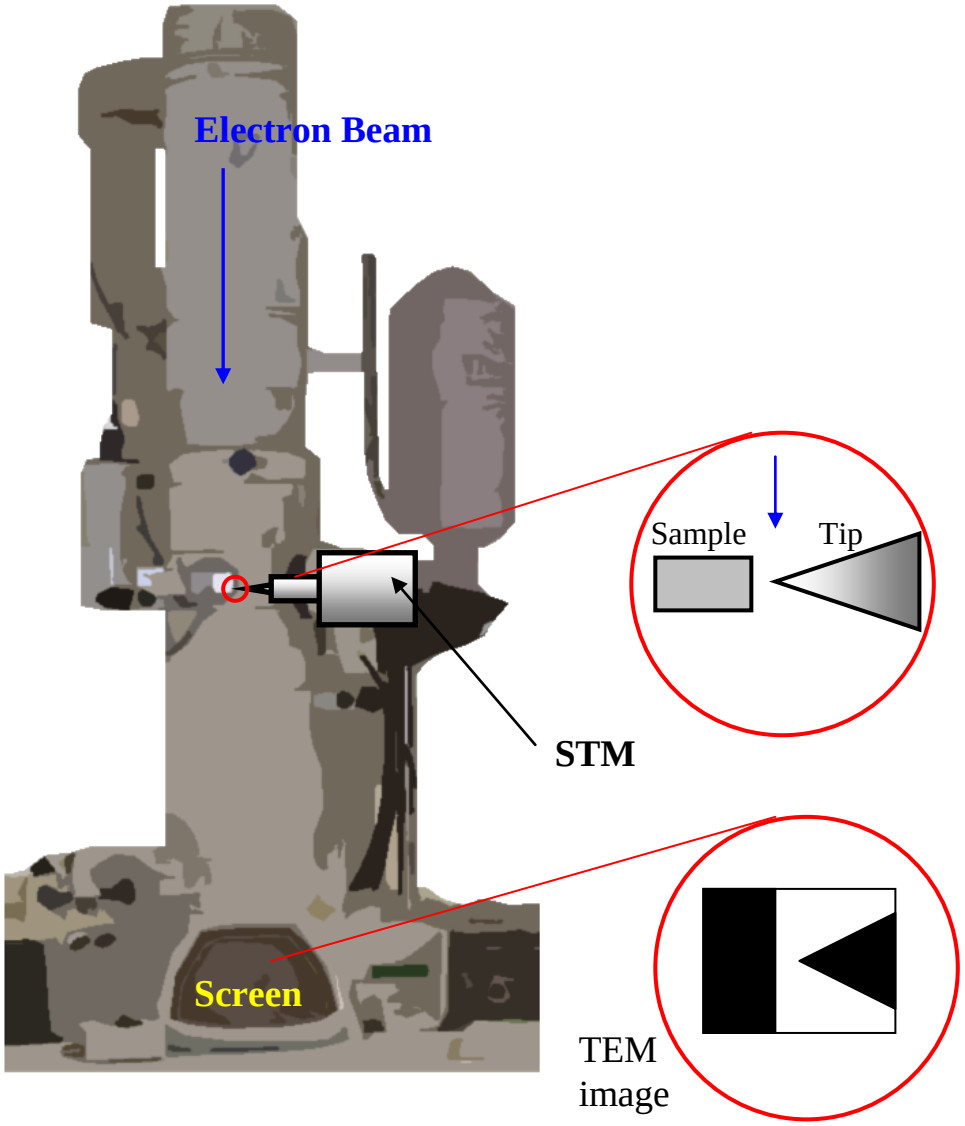

Figure 3.5: Schematic of a STM inserted into a TEM. The STM acquires electronic information about the sample and the TEM may produce an image of the tunnelling junction.

Given the multitude of different holders available for in-situ TEM investigation and that this thesis is only concerned with in-situ STM, it is this technique that will be explored in the greatest detail. In-situ STM, in a TEM, not only allows observation of both the tip and sample during STM applications, via the TEM, but also provides advantages that are not granted by standard STM techniques. Consequently, in-situ STM imaging will allow the STM tip shape to be dynamically monitored and any

changes in the tip structure (e.g. the transfer of material from the sample to the tip) could be correlated with the acquired STM images to aid understanding. In addition, the STM tip can be directed to regions of interest (i.e. lattice defects or specific nano-objects) quickly and easily using the TEM for guidance, which is preferable to finding a region of interest by repeated STM scanning. With regards to STM manipulation (see section 1.4.2), one can envisage the correlation of the trajectory of the manipulated nano-objects with the STM data providing more information on the mechanisms involved in STM manipulation events. Given that TEM provides information about the bulk properties of a sample (as electrons are transmitted through the sample) and STM gathers data on the surface structure, simultaneous acquisition of both sets of data may provide a more comprehensive examination of a sample - the two technologies are truly complementary. In addition, other TEM functions such as EDX and EELS may also be performed, for example, to determine the composition of the surface/tip, locate adsorbate atoms and observe oxide layers.

Recent studies have made progress with regards to in-situ STM. Takayanagi et al.[29] constructed a miniaturised STM that attaches to the inside of a standard sample holder. Tunneling was initiated, in-situ, and an image of gold on silicon was obtained. More recently, a commercial STM sample holder, designed for TEM, has been constructed by NanoFactory. Its design can be seen here[28]. A photograph of the holder is shown in figure 3.6. Use of this holder has led to a few interesting in-situ STM applications[30, 31].

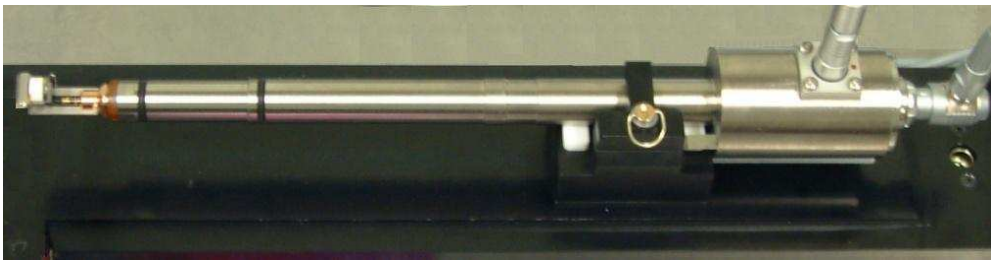

Figure 3.6: Photograph of the NanoFactory STM holder.

An experiment I conducted at the University of Nottingham illustrates a few advantages associated with in-situ STM, using the NanoFactory STM. A tungsten STM tip was positioned on a single carbon nanotube, via TEM guidance (figure 3.7a). Application of a 120V bias to the STM tip caused the carbon nanotube to fuse to it (b). The tip and

attached nanotube were then withdrawn causing the nanotube to break, leaving a nanotube strand attached to the end of the STM tip (d). This experiment illustrates the ease in which a TEM can locate a specific object of interest, such as a carbon nanotube, and observe the structure of a specific nanotube whilst simultaneously guiding the STM to its location to obtain electrical information.

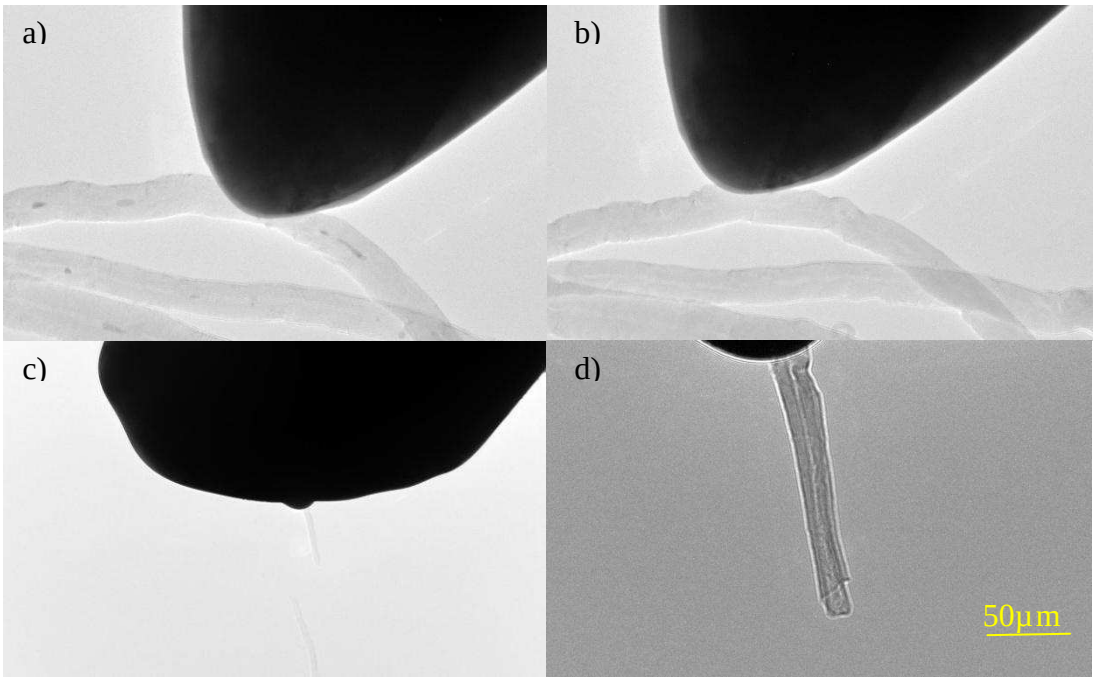

Figure 3.7: In-situ experiment using NanoFactory STM holder inside a JOEL 2100F TEM at Nottingham Nanoscience and Nanotechnology centre.

Chapter 4:

Construction of in-situ STM

4.1. In-situ Design

The main consideration in the design process was to construct a STM which is compatible with the JEOL 2010F TEM, without making any compromises that could degrade STM performance. The STM is required to be compact, due to the spatial confines of operating inside a TEM. This compact nature lends itself to a high resonant frequency - one of the most desirable critieria for an STM[32]. To maximise the resonant frequency further the chassis of the STM was constructed of rigid stainless steel – type 304. All other materials used in the construction of the STM, such as phosphor bronze and macor, were selected for their properties of high ridigity, density and, in a bid to reduce

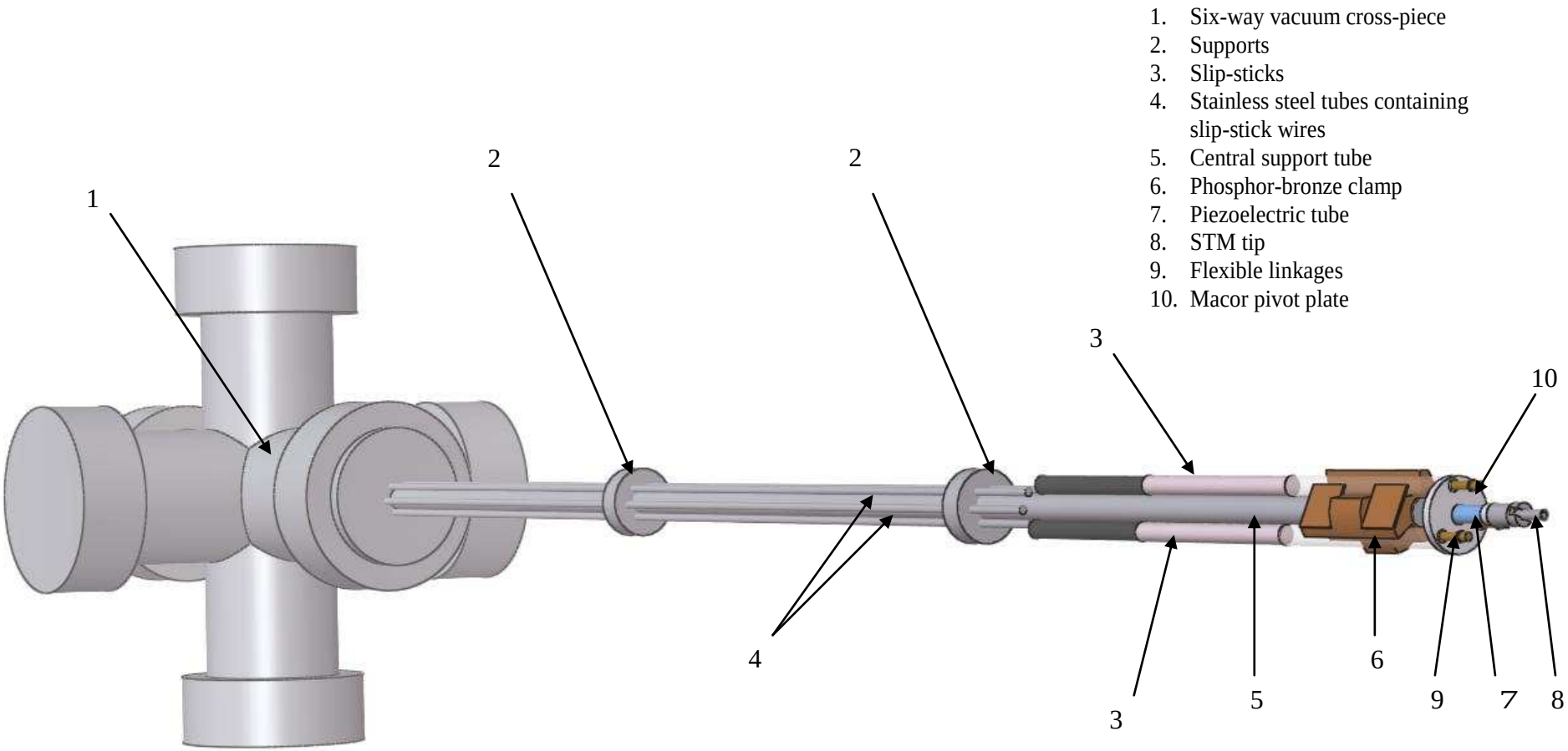

Figure 4.1: Schematic of the STM showing its internal mechanisms

thermal drift - low coefficients of thermal expansion. Furthermore, the microscope was also designed to be as symmetrical as possible to ensure only uniform thermal expanison – this will reduce the thermal drift fluctuations inherent in room temperature STM[33].

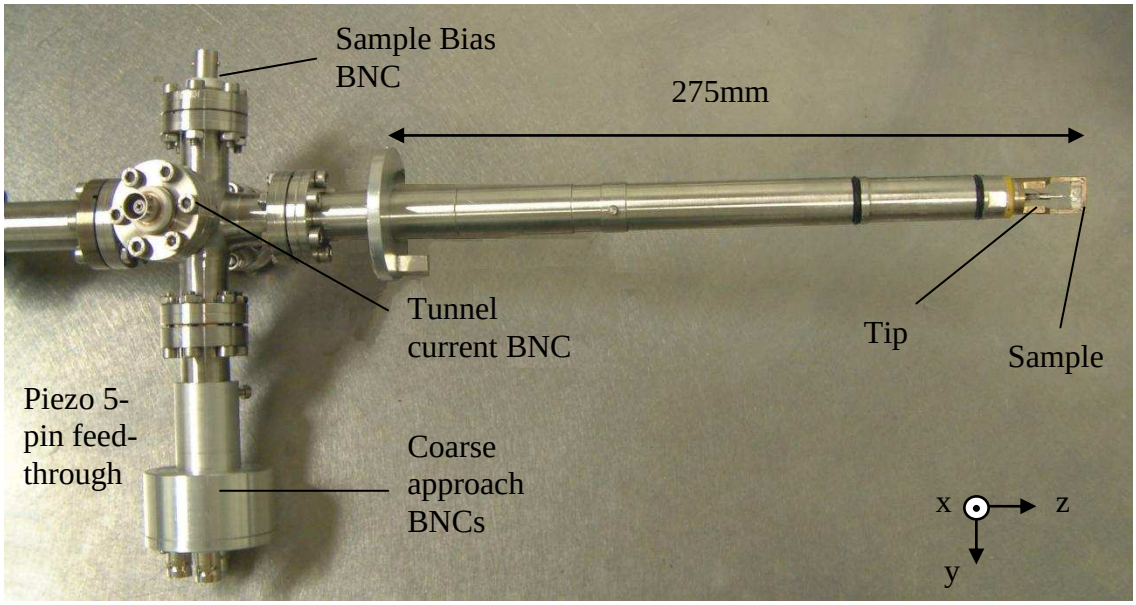

Figure 4.2: Photograph of the STM with external casing attached; ready to be inserted into the TEM.

A schematic of the new in-situ microscope is shown in figure 4.1. It consists of a six-way stainless steel cross-piece (1), in which five BNCs are attached: three BNCs are connected to the coarse approach mechanism, one is connected to the sample bias and used to apply a voltage during scanning, and one is connected to the tip and externally to a preamplifier to detect the tunnel current; a five pin feed-through connected to the piezoelectric tube (7) is also attached. Electrically connected to the BNCs are wires that run through the length of the STM. The wires that make electrical contact with the slip-sticks are kapton coated copper wires (0.24 mm OD) and are contained within stainless steel tubes (1 mm ID) (4). These wires make electrical contact to the slip-stick electrodes (3) via vacuum compatible conductive epoxy. The slip-sticks are held in place via a phosphor bronze clamp (for more information regarding the coarse approach mechanism see section 4.1). A 3 mm OD stainless steel central tube (5) is also attached to the six-way cross-piece; it acts as a central support for the STM and contains all of the wires that are connected to the tip assembly (i.e. the piezoelectric tube electrode,

tunneling current and sample bias wires – figure 4.3). These wires are also made from kapton coated copper, but have a considerably smaller outer diameter (0.14 mm), due to limits on the available volume close to the tip of the microscope. The wires attached to the piezoelectric tube electrodes are fixed in place with non-conductive epoxy as they emerge from the central support tube, where they are electrically contacted to even finer PTFE insulated copper wires (0.075 mm OD). The PTFE wires travel through small holes in the macor pivot plate (10), and make electrical contact to the corresponding piezoelectric tube quadrant (7). The sample bias wire simply runs around the macor plate and is electrically connected to the sample (11). The tunneling current wire consists of a twisted pair of kapton coated wires, one of which is grounded, and it travels through a 1 mm hole in the centre of the macor plate (10), through the central axis of the fine piezo, and makes electrical contact to the STM tip (8).

Figure 4.2 shows the STM with the stainless steel outer casing on. The outer casing is the 275 mm region shown in the figure and it essentially sheaths onto the end of the STM in figure 4.1. Its purpose is to exactly mimic the outer dimensions of a standard 2010F TEM sample holder – allowing insertion inside the TEM. The casing also holds the sample to be investigated (11).

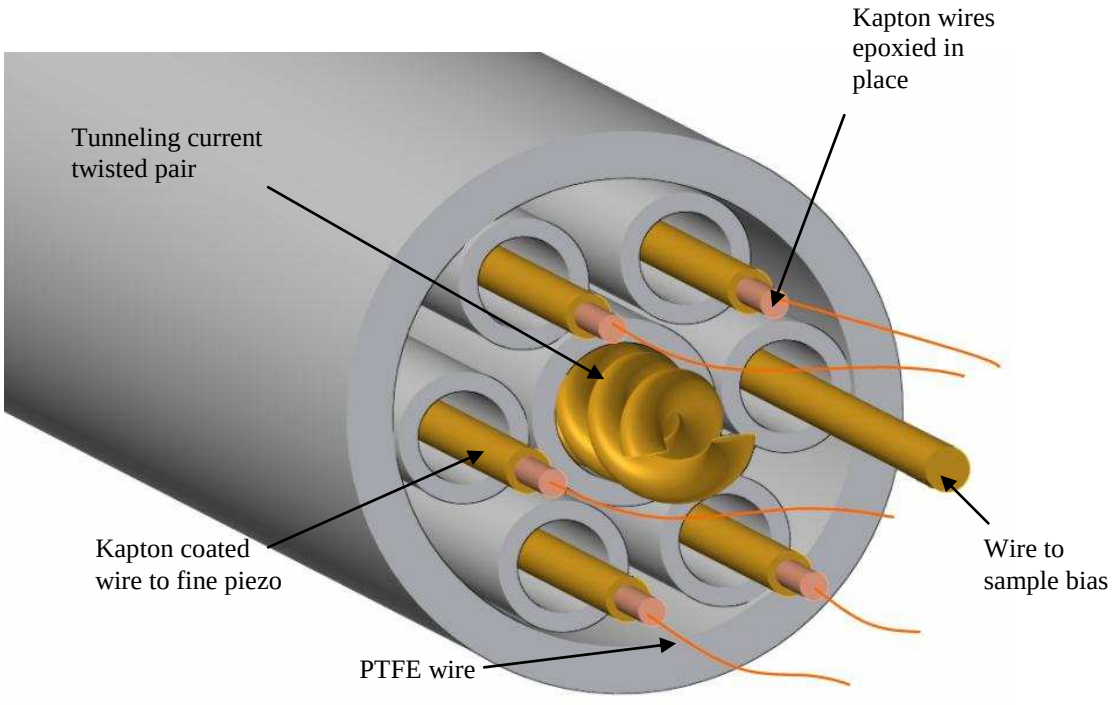

Figure 4.3: Layout of the central support tube - figure 4.1 (5). It contains seven inner tubes for electrical shielding purposes.

4.1.1. Coarse approach mechanism

The most problematic system to develop was the coarse approach mechanism, due to the difficulty in creating it within a 13 mm diameter. A novel mechanism, using inertial sliders, was designed and implemented to overcome these spatial constraints.

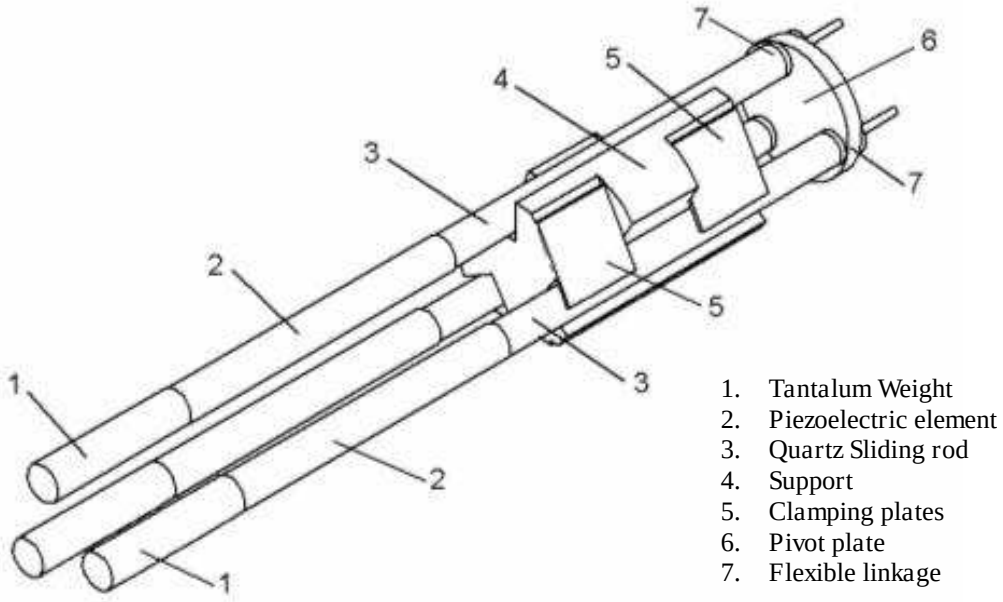

Figure 4.4: Schematic of the coarse approach mechanism

The design is based upon a hammer-action piezoelectric drive (see section 2.5.1 for more information on inertial sliding mechanisms), introduced by Welland et al.[3]; consisting of a tantalum weight – figure 4.4 (1), a piezoelectric transducer (2), and a quartz rod (3). Three of these drive units are supported, parallel to each other, within grooves machined on the circumference of a phosphor bronze central support (4). This support contacts the quartz region of the drives - leaving the piezoelectric transducers and weights unsupported. Phosphor bronze and quartz were chosen because of their low coefficients of both static and kinetic friction[34], allowing smooth motion between the rods of the drive unit and the grooves. The quartz rods are held in place with the use of clamping plates (5), which fix the rods in position and prevent any unwanted movement. At the end of the three quartz rods a plate is attached via flexible linkages (7), so that the plate may pivot on the ends of each of the sliding rods. Thus, by simultaneously applying identical voltages to all of the piezoelectric drives, the plate may be moved towards or away from the central support. However, by driving only selected piezoelectric drives, the plate can be tilted to a desired angle (with a maximum

range of approximately 30 ° from the z-axis). Using this novel mechanism the STM tip has 3 degrees of freedom of movement and can be positioned towards any regions of interest on the sample, under TEM guidance.

The total z-directional (see figure 4.2 for directional axes) range using this positional system is governed by the length of the quartz rod (3) subtracted by the length of the clamped region - providing a value of 10 mm; this is sufficient to position the tip in close proximity to the sample. However, for the tip assembly to be capable of moving 10 mm there must be a mechanism to allow for the extension and retraction of the wires that are fixed to the tip assembly. The wires that are connected to the slip-stick electrodes are deliberately loosely attached. Thus as the slip-sticks move the tip assembly forward, the wires tighten and are pulled through their stainless steel tubes (figure 4.5a). As the tubes have an inner diameter of 1 mm, it allows the wires (0.24 mm OD) to safely move up and down without causing abrasion. However, the wires that are connected to the tip assembly are much thinner due to the lack of room in this region. Initial tests illustrated that movement of the tip assembly caused severe abrasion of the kapton coating of these smaller wires, creating electrical shorts to the outer chassis. To overcome this, a new method was employed. By fixing the kapton coated wires in place to the central support tube (figure 4.3) and electrically contacting the ends of the kapton wires to very fine PTFE wires (0.075 mm OD), via conductive epoxy; the movement of the wires is contained within a much smaller region (figure 4.5b). Therefore, as the tip assembly is moved away from the clamp by the coarse approach mechanism, the PTFE wires tighten; when it moves in the opposite direction, the wires relax. Using these two methods the coarse approach mechanism can position the tip to any region in the 10mm range without causing the STM to fail.

Figure 4.5:

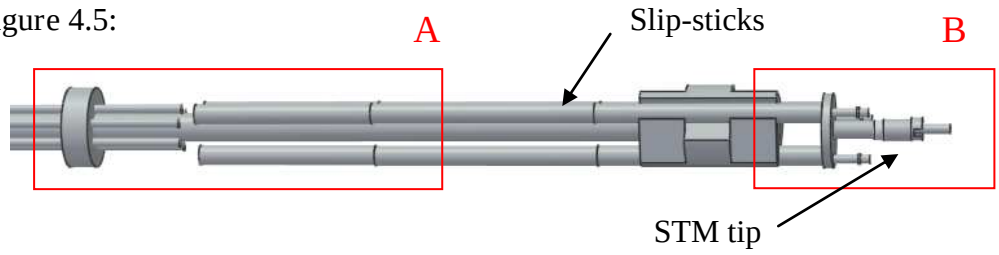

As the coarse approach mechanism moves the tip assembly towards the sample (i.e. in the z-direction) two methods are employed to allow for the extension of the wires that are fixed in position to the tip assembly. See A and B overleaf:

A

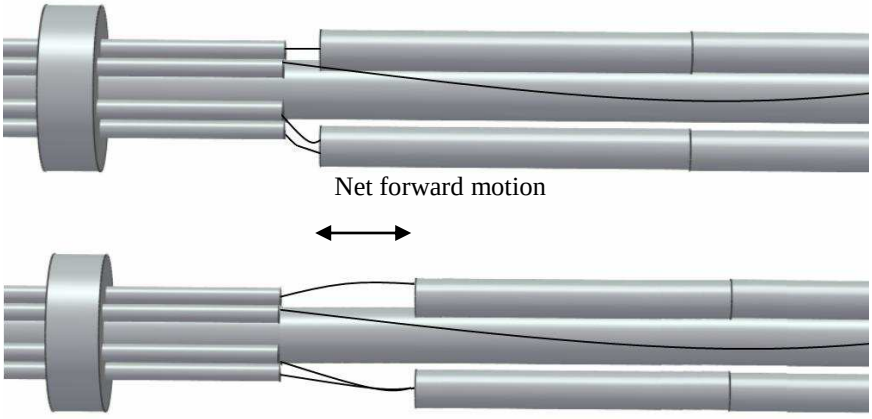

a) The slip-stick wires are pulled through stainless steel tubes, which essentially act as bearings, as the slip-sticks move the tip assembly forward.

B

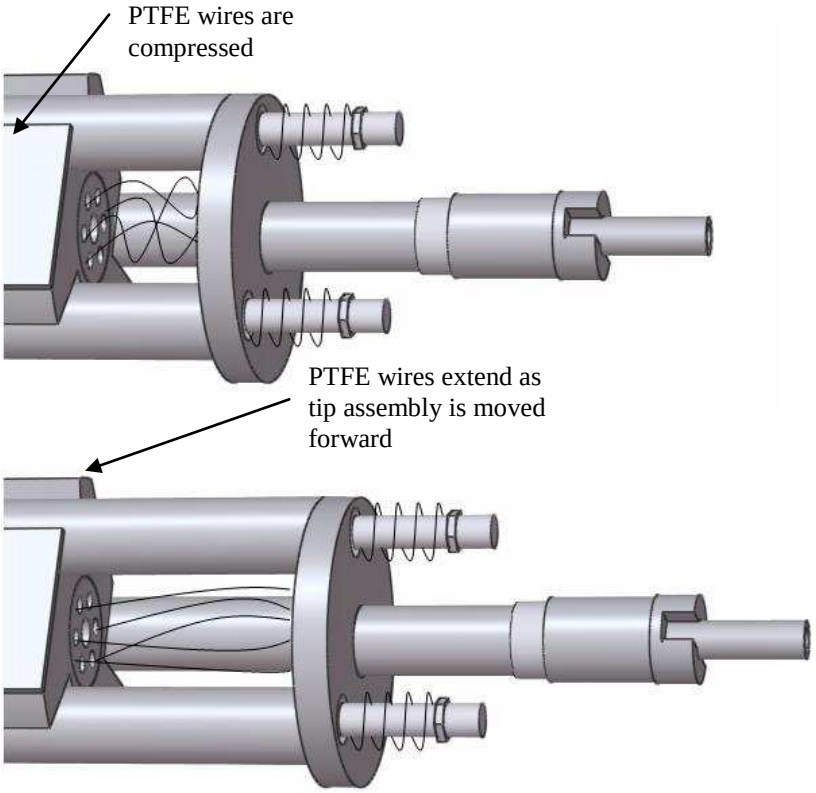

b) The fine piezoelectric wires compress and extend as the tip assembly is moved backwards and forwards respectively.

4.1.2. Fine positional mechanism

Fine motion of the STM is achieved using a piezoelectric tube, the same design as shown in section 2.5.3, of dimensions 4.5 mm length, 2 mm OD and 1 mm ID. When 150 V potential difference is applied to the inner and respective outer electrodes, the tube extends by a range of ~ 500 nm in the z-direction and 1 μm in the x and y-directions – investigated via in-situ testing. Typically voltages in the range -75 to 75 V are used - as the voltage/displacement dependence is linear in this region[23]. However, even at the maximum 150 V, with the piezo mounted within the TEM, approximately 2 mm from the electron beam, there was no degradation of the TEM image and no perceivable cross-talk with the tunneling current detection circuitry.

4.1.3. STM electronics

The STM control electronics used for the in-situ STM was supplied by Nanograph systems[35]. The control system is fully digital, based on Texas instruments TMS3206701 digital signal processor. It has 16 independent, user-programmable 16 bit A/D and D/A channels with sample rates up to 100 kHz, x, y and z drive voltages up to ± 150 V, noise levels <2 mV for 10 kHz bandwidth. The pre-amplifier used to amplify the tunnelling current signal was created in-house at the University of Nottingham; a co-axial cable connects the tunnelling current wire to the pre-amplifier, which is housed inside a shielded metal frame. Noise levels of ~ 0.01 nA were achievable using these electronics.

4.1.4. STM electrical shielding

In STM, it is paramount to ensure that not only is the instrument not susceptible to external mechanical vibrations, by ensuring a high resonant frequency and isolating it from its environment, but also that the microscope is shielded from external electrical noise[36]. The latter was achieved using a variety of methods. Firstly, the kapton wires that make electrical contact with the slip-sticks are contained within grounded stainless steel tubes. In addition, each of the wires in the central support tube is located within a grounded stainless steel tube (0.5mm ID). These grounded tubes are present to minimise the inductive and capacitance coupling between the all of the wires that are contained within the STM. The most sensitive wire in the STM is the tunneling current wire; any cross-talk will have a large effect on the small currents (~ a few nA) it

transports. This may result in a small signal-to-noise ratio, possibly degrading STM performance. Therefore, a twisted pair of kapton coated wires was employed, in addition to the twisted pair being contained within an earthed stainless steel tube. One of the wires in the twisted pair was earthed to provide extra shielding for the sensitive tunnel current wire. Also, a low-noise pre-amplifier is connected directly onto the tunneling current BNC output. Here the tunneling current is amplified to current levels that will not be as sensitive to external electrical noise – improving the signal-to-noise ratio.

4.1.5. Vacuum considerations

For simultaneous acquisition of both STM and TEM data, the STM must be able to maintain high vacuum conditions (~ $4x10^{-5}$Pa) - necessary to operate inside a TEM. Accordingly, all materials used in the STM were non-volatile, and adhesives were vacuum compatible epoxy resins[37]. The BNCs and the STM assembly are all connected to the six-way cross-piece via vacuum feed-throughs with mini conflat flanges (~25mm OD) in order to maintain excellent vacuum conditions. The STM chassis was also made entirely from stainless steel, type 304, chosen for its excellent vacuum properties[38]. With these considerations implemented, the STM was compatible with the required vacuum on a regular basis.

4.2. Performance of the in-situ STM

4.2.1. Coarse approach testing

A test was conducted to observe whether the inertial drives, of the coarse approach mechanism, were able to function in vacuum conditions. Although the inertial drives operated well at room temperature and pressure, operating inside a vacuum environment can cause problems for the inertial drives – a water layer coating the drives and clamping mechanism may aid slip-stick motion. An exponential voltage waveform, of ±150 V amplitude and 15 ms duration, was applied in-situ to the inertial drives and the STM tip was observed. A TEM image of the STM tip was obtained before and after the application of the waveform. Figure 4.6 shows that the inertial drives were able to operate within a vacuum environment.

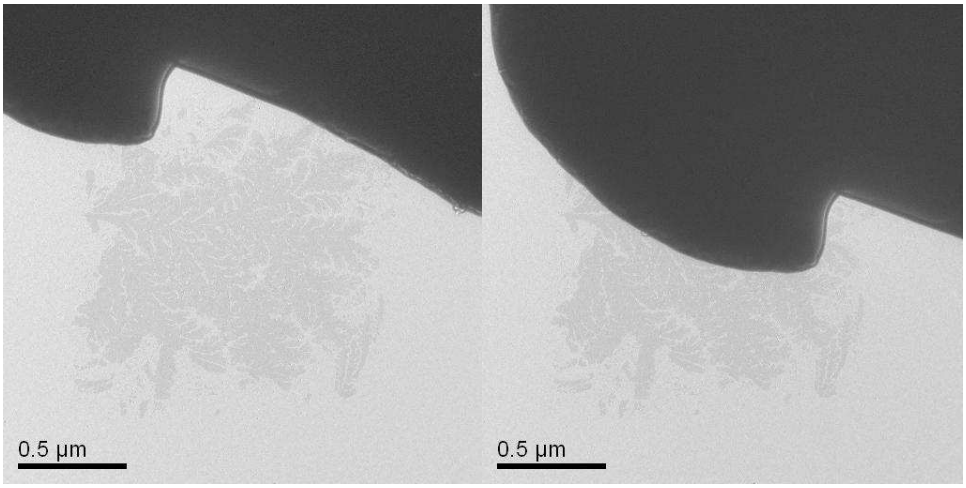

Figure 4.6: Two TEM images showing before and after a single slip-stick step, illustrating that the drives are able to perform in vacuum conditions.

The key requirement of the coarse approach mechanism is that it may be used to position the STM tip close, to within half the z-range of the piezoelectric tube. This allows the tip to be positioned close to points of interest for the fine movement control from the piezoelectric tube to be engaged - with adequate precision to avoid crashing the tip into the sample. To demonstrate the positional accuracy of the newly developed coarse approach mechanism, the STM tip was guided to a small region using only this mechanism.

Two tungsten (W) tips were electrochemically etched using NaOH solution[39] (achieving a radius of curvature of ~ 50nm). One of the W tips was mounted as the stationary STM sample, the other as the moveable STM tip. The STM holder was loaded into the TEM, and using the TEM for guidance, the STM tip was positioned as close as possible to the sample tip - using only the coarse approach mechanism. Alignment in x and z was achieved by simply guiding the tip via TEM images. However, alignment of the y-axis was slightly more difficult, because this direction is in perpendicular with the TEM images; therefore alignment was achieved by monitoring the depth of field data from the TEM.

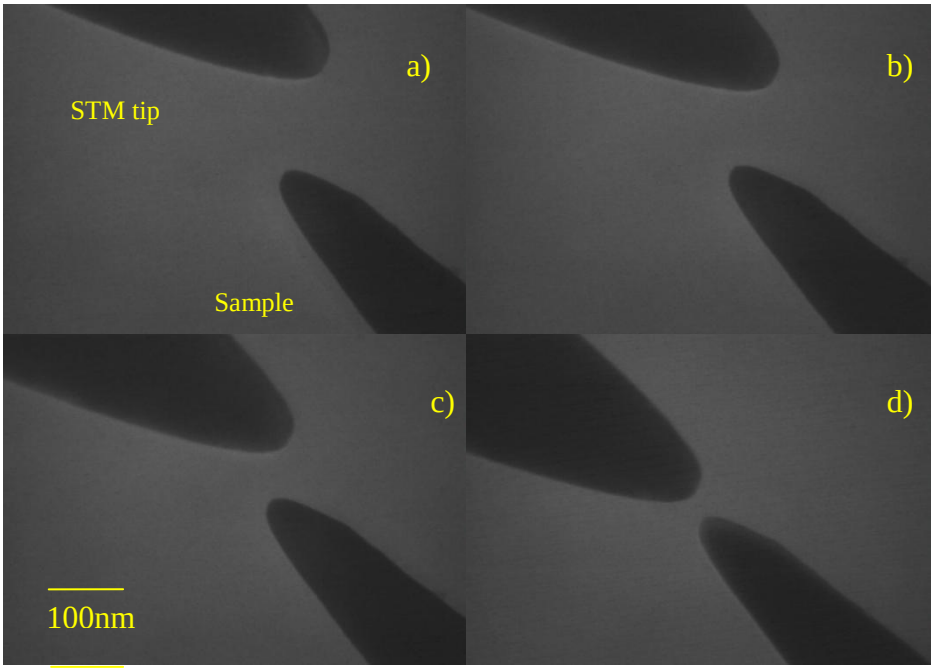

Figure 4.7: Stills taken from a TEM video showing the alignment of the STM tip to the sample tip using the novel coarse approach mechanism.

Figure 4.7 illustrates that the STM tip can be accurately positioned to within 50 nm of a region of interest using this coarse approach mechanism. This is much less than the range of the fine positional system. Therefore, using a combination of the coarse and fine mechanisms the tip can be located to any region on the sample, in 3 dimensions with sub nanometre precision.

4.2.2. Fine motion testing

Scanning was performed in-situ to observe if the electrical connections to the STM were operating satisfactorily (see section 2.5.3) and to determine the maximum scan range of the fine positional system, which was used for approximate calibration. By varying the potential applied to the x and y electrodes from 150 V to -150 V, the total range in the x and y directions were obtained. Figure 4.9 shows stills of a TEM video. From these images a maximum scan range along the x-axis of ~1 μm could be determined.

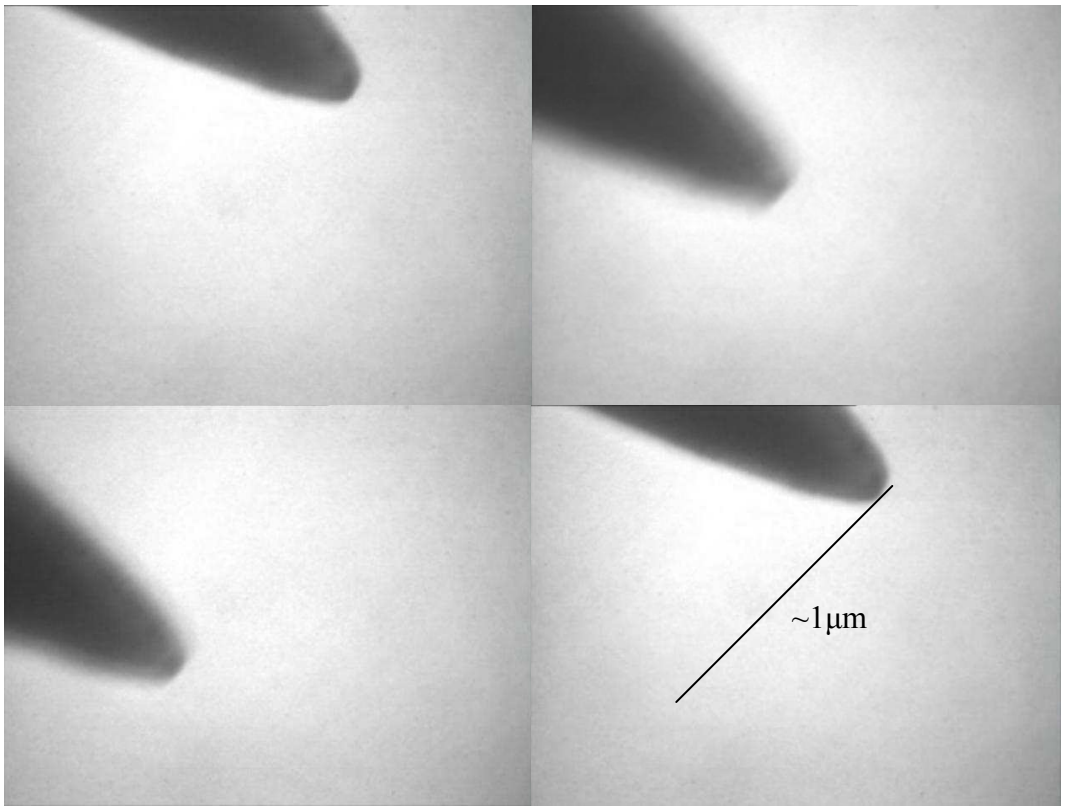

Figure 4.8: In-situ stills from a TEM video illustrating the scanning functionality of the STM. The images were also used to determine the range of movement of the piezoelectric tube in the x and y directions.

To determine the total z-range of the fine positional system, the potential difference to the outer electrodes, with respect to the inner electrode, was varied from 150 V to -150 V and images were taken of the STM tip at full extension (figure 4.9b) and full retraction (figure 4.9a). Consequently the maximum z-directional range of the piezoelectric tube could be ascertained. It was found to be ~ 500 nm.

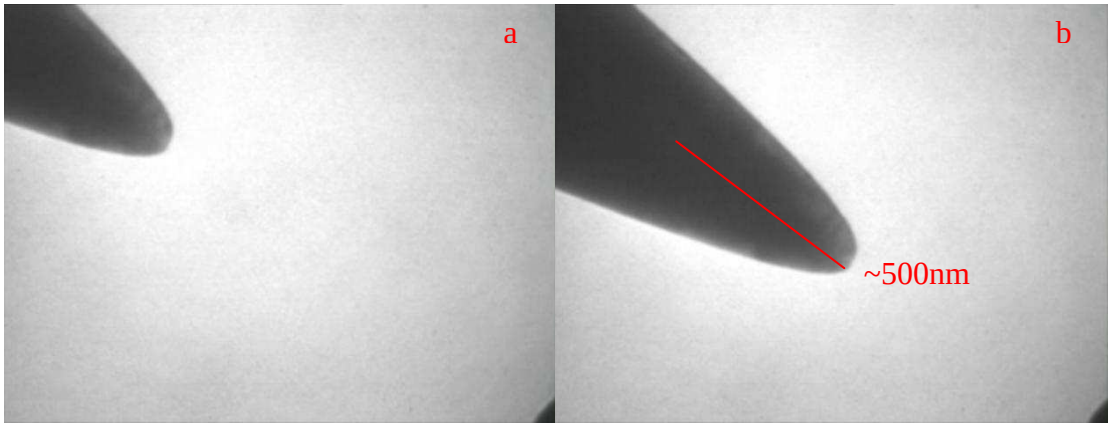

Figure 4.9: TEM images of the STM tip fully retracted and fully extended, showing the maximum z-directional range of the fine piezo.

4.2.3. Imaging

To test if the fundamental STM functions were operating correctly, ex-situ STM imaging was performed on a variety of samples at room temperature and pressure. The imaging was conducted on a passive vibration isolation table to reduce vibrations from mechanical sources. Scans were performed using mechanically cut Pt/Ir (composition 80/20) STM tips on a variety of samples. The images obtained can be seen in figure 4.10.

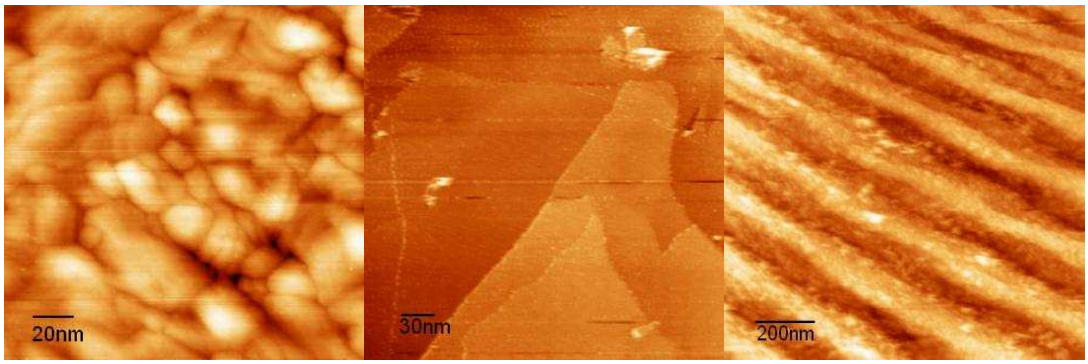

a) b) c)

Figure 4.10: Ex-situ STM images of a) gold on a silicon substrate - 0.7 nA, 0.5 V , b) graphite - 0.5 nA, 0.5 V - and c) au calibration grid, with parallel grooves - 0.2 nA, 0.5 V.

Figure 4.10a is a STM image of Au on a silicon substrate, with the image exhibiting the characteristic features expected for a polycrystalline film. Figure 4.10b is a scan of HOPG, with step edges clearly visible. Figure 4.10c is a much larger scan of an Au

calibration sample. It consists of periodic parallel lines separated by ~ 280 nm, which can be clearly seen in the image. Observation of these images seems to suggest that the STM is in operational order and confirms the electronic feedback mechanism is working, as the images show all the characteristic features of the respective samples. Also encouraging is the lack of any periodic noise in the images, suggesting the STM is adequately electrically shielded from its environment.

4.2.4. Noise Considerations

Electrical noise on the bench picked up by the tunneling current wire typically has an amplitude of ~ 0.02 nA, with a mean of ~ 0.002 nA. The noise is generally in the 50 Hz region. It is advantageous to conduct STM with a setpoint an order of magnitude greater than the maximum noise level[40]. Figure 4.10 demonstrates that the signal-to-noise ratio is large enough to resolve key features in the sample, i.e. step edges on graphite. However, when operating in-situ the noise levels raise considerably. This may be due to induced currents in the tunneling current wire due to the electromagnets in the TEM or simply due to the currents from the electron beam. In-situ noise levels are typically around a factor higher than in ex-situ STM (see figure 4.11). This may make in-situ imaging more troublesome, requiring a setpoint of ~3nA to produce an adequate signal-to-noise ratio.

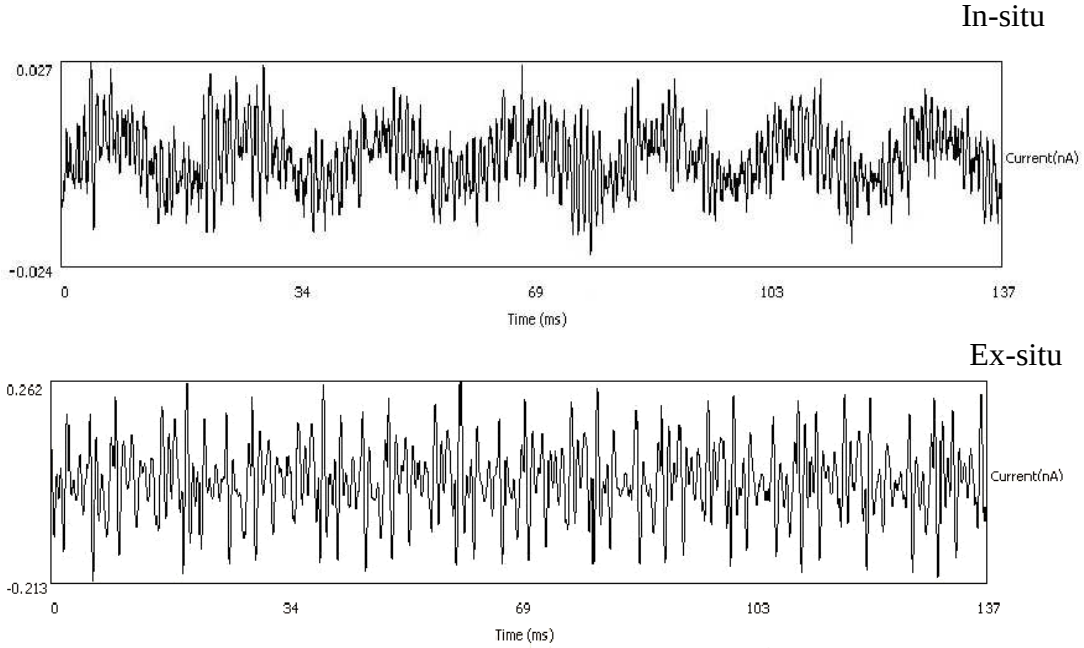

Figure 4.11: Noise data for STM in-situ and ex-situ.

4.4. Summary

This chapter has provided information on the design and operation of the in-situ STM which I have developed. A novel coarse approach mechanism has been introduced that operates in high-vacuum conditions and is able to position to the tip precisely enough for the fine mechanism to engage. Fine motion has also been observed in-situ, and through a combination of the fine and coarse approach mechanisms the STM tip has been successfully guided to another etched tungsten tip, with radius of curvature ~ 50nm. Ex-situ imaging has yielded satisfactory results, with characteristic features observed in the images. However, in-situ electrical noise has been shown to be of higher magnitude than ex-situ noise; more detailed experimental evidence is required to determine if this reduced signal to noise ratio will detrimentally affect imaging performance.

It is evident that the compromises made in the STM design, in order to meet the spatial constraints of operating in a TEM, have not drastically reduced ex-situ imaging performance. It is also clear that essential STM functions such as the coarse approach mechanism, fine approach mechanism and biasing mechanism are operational in-situ; however, further investigation is required to assess in-situ imaging performance.

Chapter 5:

Investigation of Silver Sulphide STM Tips

5.1. Silver Sulphide

The first experiment chosen to demonstrate the dynamic properties of the STM/TEM combination was the formation of silver on the tip apex of a silver sulphide (Ag_2S) crystal. This experiment was originally conducted by K. Terabe et al. using an in-situ STM in a SEM[41]. The fundamental theory behind this experiment is related to the solid electrochemical process (see figure 5.1).

5.1.1 The Solid Electrochemical Process

Figure 5.1: Diagram illustrating the solid electrochemical process.

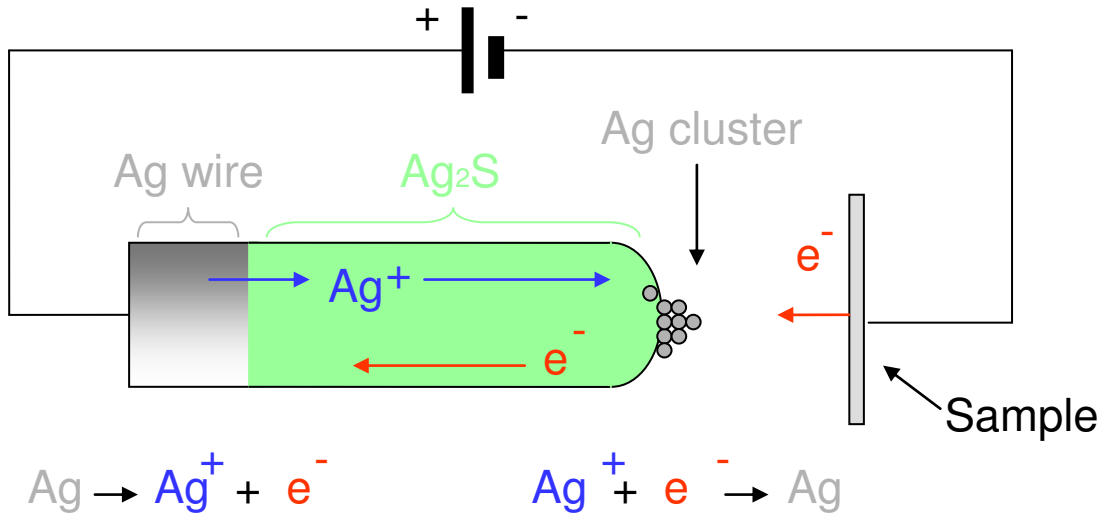

a) When a negative bias is applied to the sample, mobile silver ions travel through the sulphur lattice towards the tip apex; here they are reduced by tunnelling electrons to form neutral silver atoms. These silver atoms form a protrusion on the tip apex that grows with time.

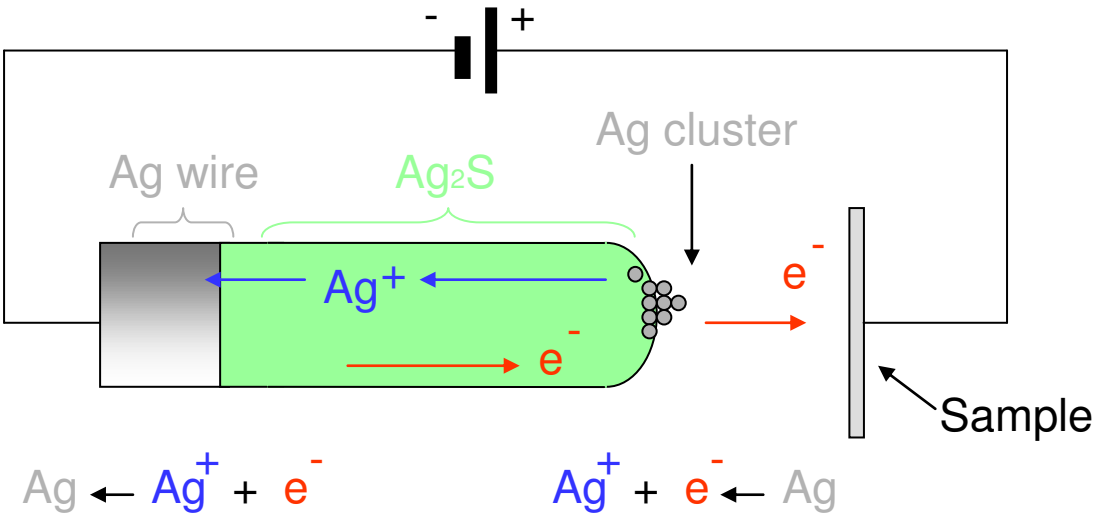

b) If the sample is positively biased the silver atoms at the tip apex oxidise and the silver ions travel back into the bulk, while the electrons tunnel to the sample. The silver protrusion therefore reduces in size with time.

5.1.2. The Production of Silver Sulphide Crystals

The process used to create these Ag_2S crystals was discussed by Terabe et al. Approximately 5 g of sulphur powder, 99.99% purity, was placed into a glass tube of 4 mm diameter and ~ 50 mm length. A 20 mm length of silver wire was also placed into a ~ 2 mm diameter capillary tube (figure 5.2a). Both these tubes were positioned within a ~ 250 mm borosilicate tube, in which the open end of the tube was connected to a vacuum scroll pump. The pressure in the tube was evacuated to $1x10^{-3}$ Pa, to remove any substances that could affect the purity of the experiment. By melting the open end of the borosilicate tube, the contents were completely sealed and the vacuum inside maintained. The sealed tube was then placed in a furnace; the silver wire was heated to 300 °C and the sulphur powder was maintained at 70°C. The tube was left for 3 days; allowing time for the sulphur powder to evaporate, diffuse across and chemically bond with the silver wire. After 3 days, black silver sulphide crystals were observed at the ends of the silver wires (see figure 5.2b).

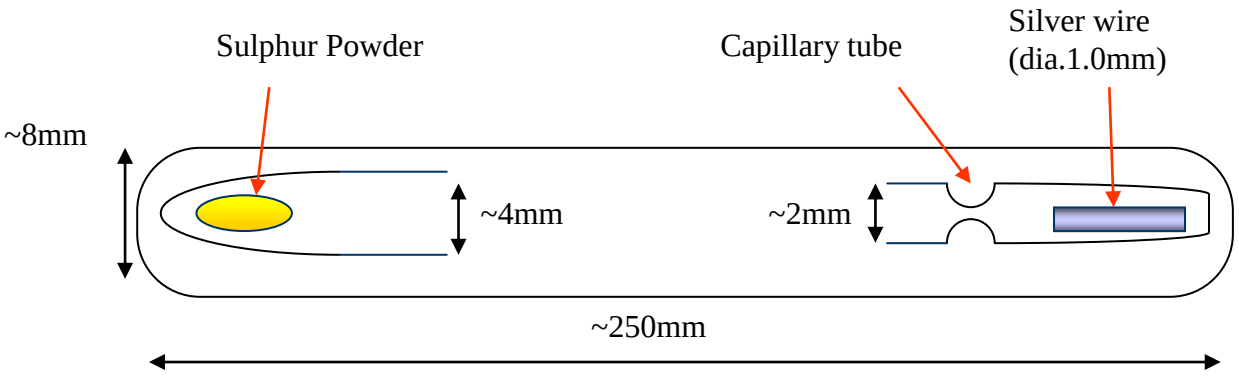

Figure 5.2a: Experimental setup used to create Ag_2S crystals

Figure 5.2b: Silver sulphide crystals grown on the apex of a silver wire (left) and a SEM image of some silver sulphide crystals (right).

To ensure that the crystals in figure 5.2b were composed of Ag_2S, EDX was performed on the crystals inside a TEM (see section 3). The results are shown in figure 5.3.

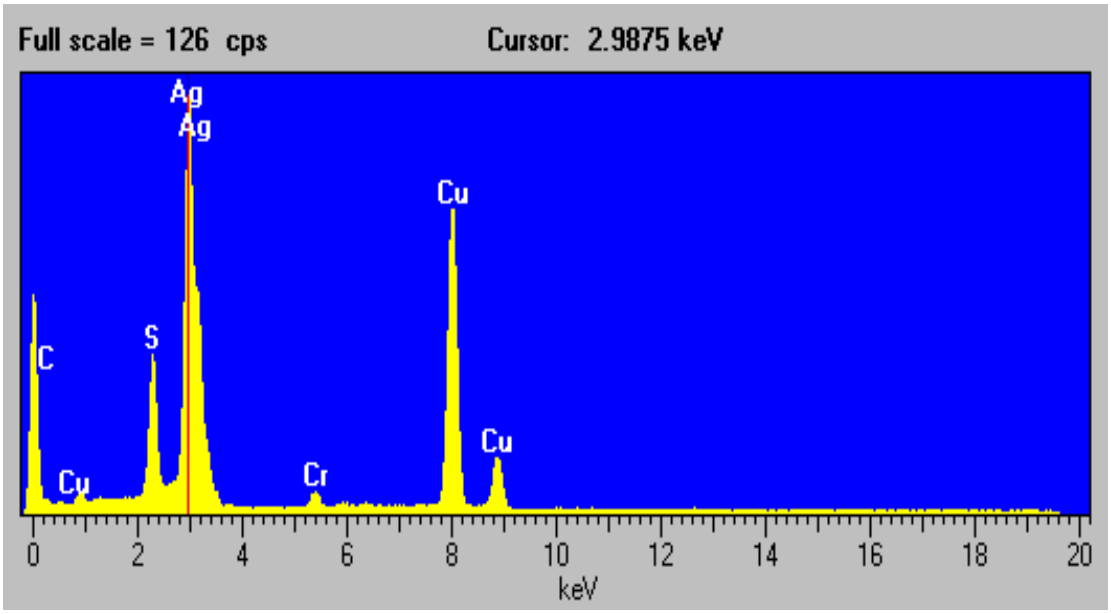

Figure 5.3: EDX analysis of the crystals created in figure 5.2. The graph shows a composition of 71% silver and 29% sulphur; a ratio of 2:1 (Ag:S) is theoretically expected from Ag_2S. Cu is also observed as the sample was placed on a copper TEM

sample grid. Carbon and chromium are also observed due to impurities in the TEM chamber.

The dynamic nature of the solid electrochemical process was identified as a possible route for investigation using the STM/TEM combination, in particular in relation to in-situ manipulation experiments. This approach would make use of a Ag_2S tip as a local source, or sink, of Ag which would be deposited on supported nanostructures which might potentially act as a reversible bond. In order to investigate the feasibility of this approach the Ag_2S crystals were investigated using SEM and TEM.

5.1.3 Analysis of Silver Sulphide in SEM

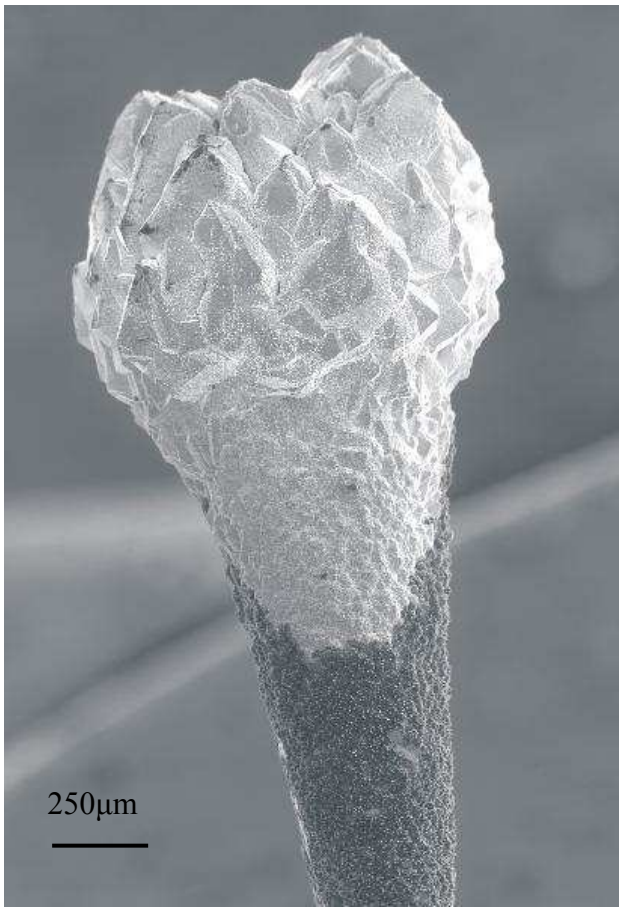

Figure 5.4: SEM of a Ag_2S tip.

The Ag_2S crystal exhibited no changes when the SEM electron beam scanned a large area (figure 5.4). However, as the electron beam scan area was reduced, to ~ 20 x 20 μm, small growths started to protrude from the surface of the crystals, almost immediately (see figure 5.5).

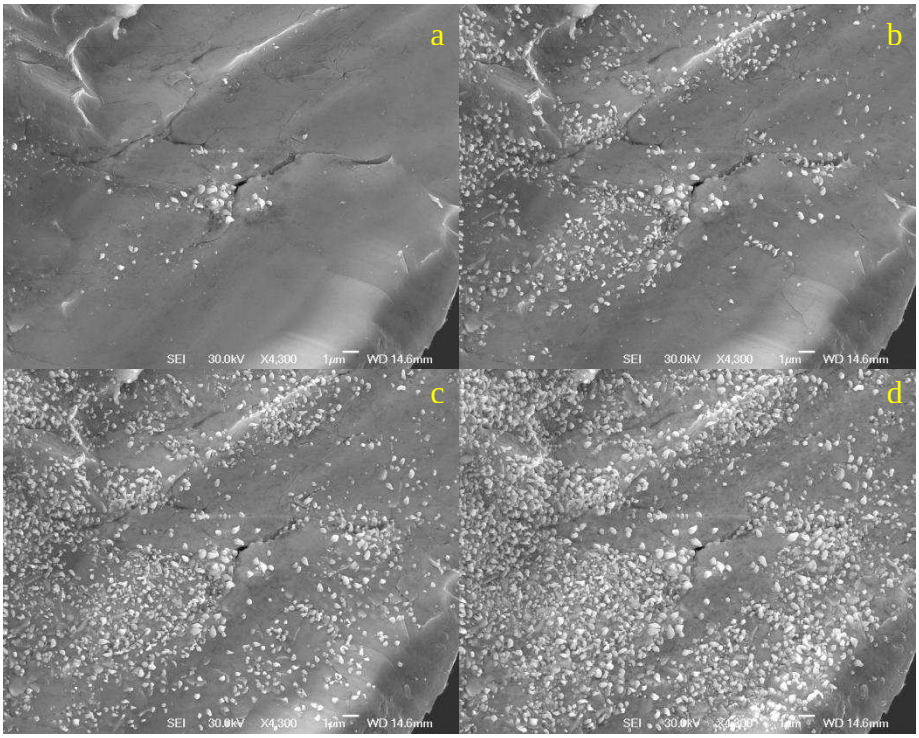

Figure 5.5: a-d) SEM images illustrating the continual growth of protrusions using the SEM electron beam with increasing exposure of the electron beam.

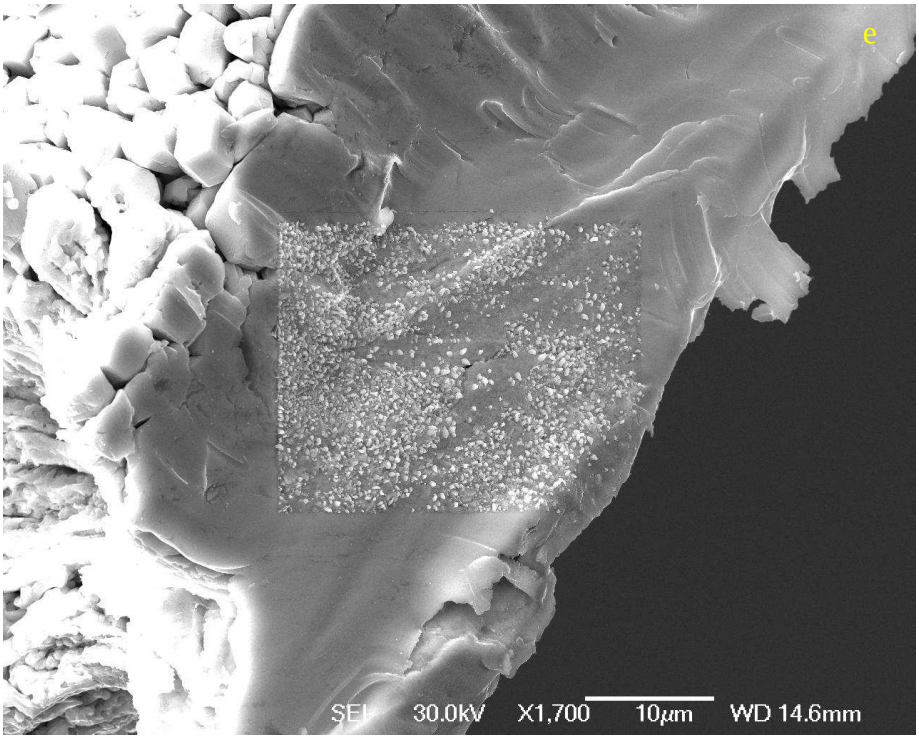

e) A ~ 70 x 55 μm SEM image, showing a clearly defined rectangle of grown protrusions of the previous images.

In figure 5.5, where the electron beam is only covering a small area (a), the Ag_2S surface deforms, with protrusions growing in size on the surface. The longer the surface is exposed to the beam, the more growths emerge and the larger the initial protrusions grow (b). However, the amount and size of the protrusions saturate after a certain time - no more growth occurs (d). The growth of these protrusions is entirely dependent on the area exposed to the electron beam, as when the field size is increased (e) no more protrusions are grown. To investigate why and how these protrusions are grown, an experiment was conducted to determine the voltage dependence of their formation.

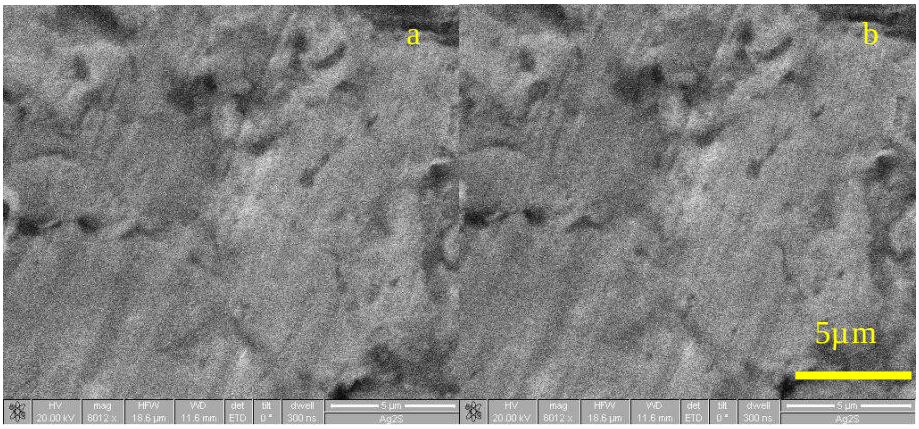

Figure 5.6: SEM images of Ag_2S taken while SEM beam is zoomed in but only has an electron beam voltage of 15kV

In figure 5.6, the electron beam field size was ~ 18 x 16 μm but the electron beam voltage was reduced to 15kV, half of that in figure 5.5. A SEM image was taken (a). The beam was left for approximately 60 seconds and the second image was taken (b). At this voltage there were no protrusions grown on the Ag_2S, this suggests that the protrusion growth is voltage dependant.

The mechanism behind the growth of these protrusions may be explained by the solid electrochemical process, figure 5.1. The electron beam incident on the Ag_2S surface may cause mobile silver ions travel to the surface, which are reduced to form neutral silver protrusions. To determine whether this is the case, protrusions were grown from the surface using a beam voltage of 20kV. EDX was performed on these protrusions to determine the composition.

a) b)

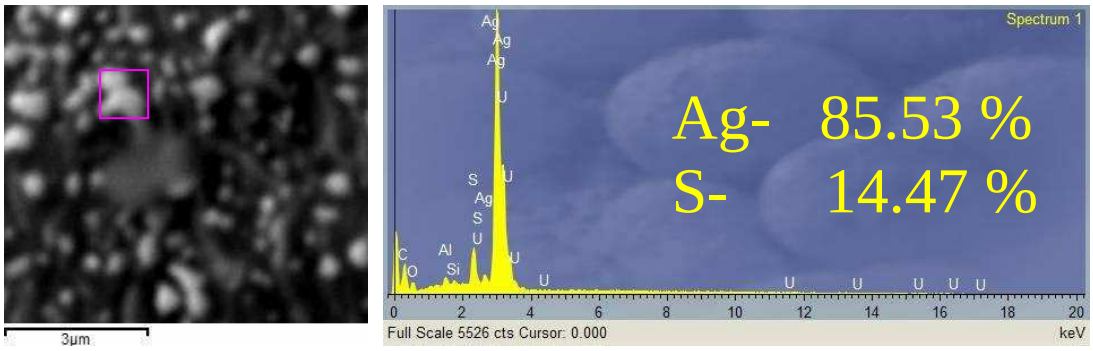

Figure 5.7: a) SEM image of a region of Ag_2S surface, the purple square indicates the region the EDX was performed on. b) The EDX spectra of the purple region.

b)

Figure 5.7 illustrates that the chemical composition of the protrusion is 85.53 % silver and 14.47 % sulphur. This data suggests that the protrusion contains a higher ratio of silver than Ag_2S. This increase in the ratio can be explained by assuming the protrusion is made of silver. This assumption is backed up by the following evidence.

a) b)

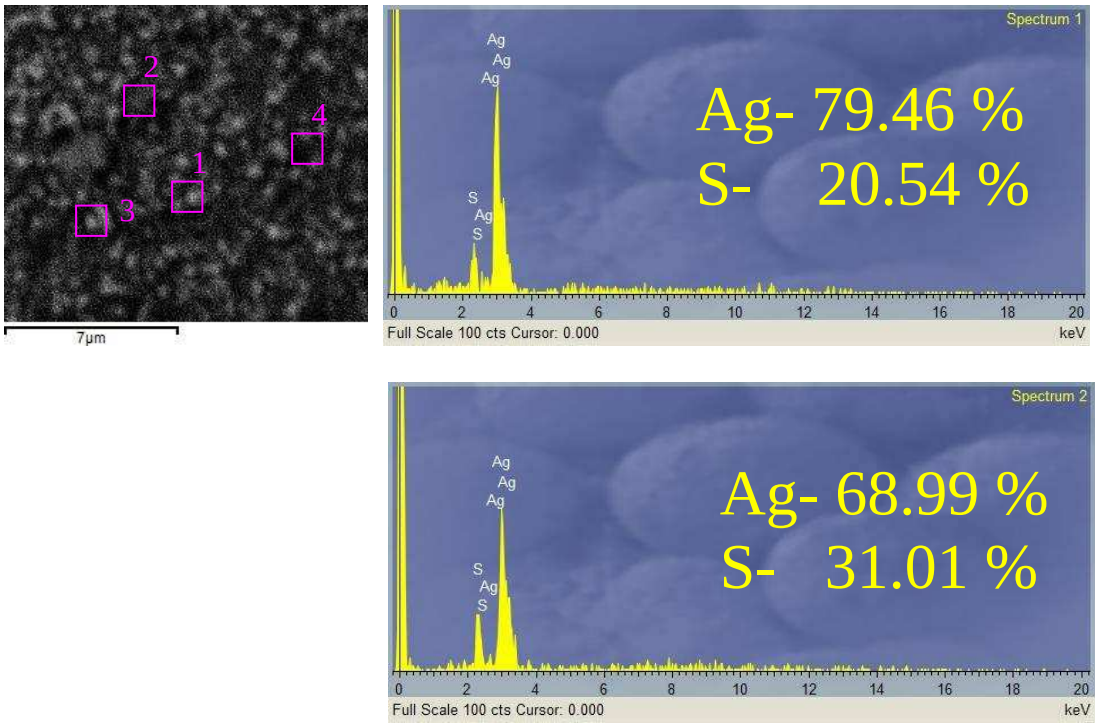

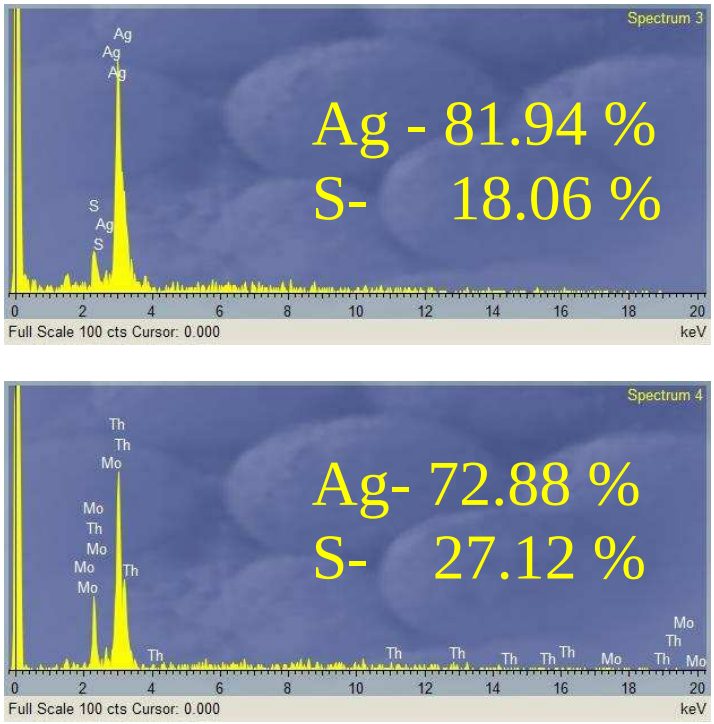

Figure 5.8: a) SEM image of a region of Ag_2S, the purple areas are the regions EDX was performed on. b) The EDX spectrum of the areas shown in a), percentage composition of Ag and S is also shown.

Figure 5.8a illustrates that areas 1 and 3 were located over a grown protrusion; areas 2 and 4 are not. The corresponding EDX spectra, in figure 5.8b, show that regions 1 and 3 have a larger concentration of silver; regions 2 and 4 have the same ratio of silver as Ag_2S. EDX spectra were obtained for, in total, 20 regions located both on protrusions and not on protrusions. The average percentage silver concentration for regions on these protrusions was 79.44%; compared to an average of 69.64% for regions not located on a grown protrusion. This suggests quite conclusively that the protrusions contain a higher percentage of silver than standard silver sulphide; providing more evidence that these protrusions were formed by the solid electrochemical process, described in figure 5.1.

5.2. Summary

The experiments conducted on Ag_2S illustrated that the crystals have very limited lifetime in a TEM and this material was not well suited to the manipulation experiments previously discussed. This is primarily because the growth of the silver protrusions will not be dominated by the tunneling current, but by the TEM electron beam current. However, the physics of how these protrusions grow is as yet not fully understood and merits further investigation. Future experiments may be conducted to observe if the size and rate of growth of these protrusions are functions of voltage and beam current. Also, it is clear that the silver protrusions do not uniformly distribute across the surface; the physics of why this occurs may be explained in terms of lattice imperfections and dislocations[42]. If lattice imperfections of Ag_2S could be correlated to the distribution of the silver protrusions, more information about the mechanism of the solid electrochemical process in Ag_2S may be obtained. The information obtained from these possible experiments may allow limited control of how these protrusions grow which may lead to possible future applications.

Chapter 6:

6.1 Conclusion

The work in this thesis has been primarily focused on the research and development of a novel STM that is compatible with a JEOL 2010F TEM. The overall performance of the STM has been investigated. Experiments performed in-situ illustrate that the STM is able to operate within the confines of a TEM. The novel coarse approach mechanism, unique to this STM design, has been observed to have the required mechanical stability and was able to precisely position the STM tip to a region of interest of approximately 50 nm; close enough for the fine approach mechanism to engage. Ex-situ testing has demonstrated that the fundamental functions of the microscope are operating satisfactorily and images have been acquired. The microscopes design and construction has been fully completed and is ready for use in experimental procedures.

The potential benefits of in-situ STM have also been discussed, and possible applications suggested. One such application has been investigated in detail: in-situ STM manipulation using silver sulphide crystals. While it has unfortunately proven unachievable with application to in-situ use, some interesting physics has been revealed in relation to the formation of protrusions when bombarded with electrons.

References

[1] G. Binnig, H. Rohrer, Ch. Gerber and E. Weibel, "7x7 reconstruction of Si(111) resolved in real space", Phys. Rev. Lett. 50, pp.120-123 (1983)

[2] http://www.fz-juelich.de/video/emundts/film.mpg

[3] C. N. Woodburn, A. W. McKinnon, D. A. Roberts, M. E. Taylor and M. E. Welland, "A one-dimensional piezoelectric-driven inertial micropositioner with vertical capabilities", Meas. Sci. Technol. 4, pp.535-537 (1993)

[4] http://news.bbc.co.uk/1/hi/technology/7098005.stm

[5] G.E. Moore, "Cramming more components onto integrated circuits" Electronics magazine, pp.4 (1965)

[6] B. Gates, "Why the PC Will Not Die," Newsweek, May 31 (1999)

[7] Collins, G. Philip, Phaedon Avouris, "Nanotubes for electronics" Scientific American, Dec pp. 62-68 (2000)

[8] N Taniguchi, "On the basic concept of nano-technology", Proc. Intl. Conf. Prod. London, Part II, British Society of Precision Engineering (1974)

[9] http://www.foresight.org/grandprize.1.html

[10] G. Binnig, H. Rohrer, Ch. Gerber and E. Weibel, "Tunelling through a controllable vacuum gap", Applied Physics Letter 40, pp.178 (1982)

[11] C. J. Kiely, "Electron microscopy and analysis: Proceedings of the Institute of Physics Electron Microscopy and Analysis Group Conference", University of Sheffield (1999)

[12] G. Binnig, H. Rohrer "Scanning tunneling microscopy" IBM Journal of Research and Development, vol. 30; issue 4, pp.355 (1986)

[13] J.Bardeen, "Tunnelling from a Many-Particle Point of View," Phy. Rev. Lett. 6, pp. 461 (1961)

[14] R. Wiesendanger, "Scanning Probe Microscopy and Spectroscopy: Methods and Applications", Cambridge University Press, 1 edition, pp. 105-7 (1994)

[15] J. Tersoff and D.R. Hamann, "Theory of the scanning tunnelling microscope", Phy. Rev. Lett. B, 31, pp.805-813 (1985)

[16] C. Noguera, "An exact expression of STM tunnelling", Journal of Microscopy, Vol. 152, Pt 1 (1998)

[17] R. J. Hamers, R. M. Tromp and J. E. Demuth, "Surface electronic structure of Si(111)-(7x7) resolved in real space", Phy. Rev. Lett. 56, pp.1972-1975 (1986)

[18] D. M. Eigler and E. K. Schweizer, "Positioning single atoms with a scanning tunnelling microscope", Nature 344, pp.524-526 (1990)

[19] L. Bartels, G. Meyer and K. H. Rieder, "Basic steps of lateral manipulation of single atoms and diatomic clusters with a STM tip", Phy. Rev. Lett. 79, pp.697 (1997)

[20] T. T. Tsong, "Effects of an electric field in atomic manipulations", Phys. Rev. Lett. 44, pp.13703-10 (1991)

[21] C. Z. Rosen, B. V. Hiremath, R. E. Newham, “Piezoelectricity”, (1990)

[22] D. W. Pohl, “Dynamic piezoelectric translation devices”, Rev. Sci. Instrum 58, pp.54.57 (1986)

[23] J. A. Stroscio, W. J. Kaiser, “Scanning Tunneling Microscopy”, vol. 7, Academic Press. Inc (1993)

[24] C. Bai, “Scanning Tunneling Microscopy and its Application”, Springer, Heidelberg (1995)

[25] J. Hillier and R.F.Baker, "Microanalysis by means of electrons", J. Appl. Phys. 15, pp.663 (1944)

[26] H. Olin, F. Althoff, K. Svensson, United States Patent Application Publication, Publication no. US2004/0051424A1

[27] J.J. Wang, A. Lockwood, R. Gay, B. J. Inkson, “Characterising ambient and vacuum performance of a miniaturised TEM nanoindenter for in-situ materials deformation” , J. Phys. Conf. Proc, 126, 012095 (2007)

[28] X. Xu, A. Lockwood, R. Gay, Z. Saghi, J.J. Wang, Y. Peng, B. J. Inkson, G. Möbus, “A full tilt range goniometer inside a TEM goniometer” Proc EMC Aachen, Tomography Unlimited, 1, pp.315 (2008)

[29] H. Ohnishi, Y. Kondo and K. Takayanagi, “In-situ operation of a STM in a UHV TEM”, Microscopy and microanalysis (2002)

[30] M.L. Taheri, B. Simpkins, P. Pehrsson, R.M. Stroud, “Lift-out and In-situ STM-TEM Studies of Individual GaN Nanowires” Physical Sciences – Microscopy in Nanoscience and Nanotechnology, pp.702-703 (2006)

[31] R.M. Stroud, T.J. Zega and M.L. Taheri, “In-situ Lift-Out for Coordinated Structure-Electron Transport and Structure-Isotope Studies” Advances in Instrumentation and Techniques - FIB and FIB/SEM: Applications and techniques for Physical and Biological Sciences, pp.1266-1267 (2006)

[32] H. van Kempen, G.F. A. van de Walle, “Applications of a high-stability STM.”, IBM J. Res. Develop 30, pp.509-514 (1986)

[33] O. Albrektsen, L.L. Madsen, J. Mygind and K. A. Morch, “A compact STM with thermal compensation” J. Phys 22, pp.39 (1989)

[34] http://www.roymech.co.uk/Useful_Tables/Tribology/co_of_frict.htm

[35] http:// www.nanographsystems.co.uk

[36] Ch. Gerber, G. Bining and C. F. Quate, “Atomic force microscope”, Phys. Rev. Lett. 56, pp.930 (1986)

[37] http://www.bondline.net/properties/electric.html

[38] M. F. Ashby and D. R. H. Jones "Chapter 12, Engineering Materials 2, with corrections” Oxford Pergamon Press, pp.119 (1992)

[39] P. Bryant, H.S. Kim, Y. C. Zheng and R. Yang, “Scanning tunelling microscope tips”, Rev. Sci. Instrum, 58, pp.1115 (1986)

[40] C. J. Chen, “Introduction to Scanning Tunneling Microscopy” Oxford University Press, New York (1993)

[41] K. Terabe, T. Nakayama, T. Hasegawa and M. Aono, "The formation and disappearance of nanoscale silver cluster realized by solid electrochemical reaction", Jour. of App. Phys., Vol. 91, 12, pp.10110-10114 (2002)

[42] H. L. Tuller, "Ionic conduction in nanocrystalline materials," Solid State Ionics 131, pp.143-157 (2000)